Investigation of Electronic Communication in Multi-Porphyrin Light-Harvesting Arrays

Jyoti Seth,[†] Vaithianathan Palaniappan,[†] Thomas E. Johnson,[‡] Sreedharan Prathapan,[‡] Jonathan S. Lindsey,[‡] and David F. Bocian*[,†]

Contribution from the Departments of Chemistry, University of California, Riverside, California 92521-0403, and Carnegie Mellon University, 4400 Fifth Avenue, Pittsburgh, Pennsylvania 15213-2683

Received June 22, 1994[⊗]

Abstract: A comprehensive electrochemical (cyclic and square-wave voltammetry, coulometry) and static spectroscopic (absorption, resonance Raman (RR), electron paramagnetic resonance (EPR)) study is reported for several pentameric and dimeric porphyrin-based arrays and their monomeric building blocks. The pentameric arrays consist of a central tetraarylporphyrin linked to four other tetraarylporphyrins via ethyne groups at the *p*-positions of the aryl rings. The complexes investigated include Zn_5 pentameric and Zn_2 dimeric porphyrin arrays, a pentameric array in which the four peripheral porphyrins are zinc and the central porphyrin is a free base (Zn_4Fb_1), and a mixed zinc-free base porphyrin dimer (Zn_1Fb_1). The center-to-center inter-porphyrin distances in the arrays are ~20 Å. The dimensions of the dimeric and pentameric arrays are ~40 and ~60 Å, respectively. The spectroscopic studies were performed on singly and multiply oxidized complexes as well as the neutral species. The electrochemical and spectral properties of the arrays indicate that the electronic communication between the macrocycles is relatively weak in the ground and excited electronic states. The absorption characteristics of the arrays can be explained in terms of long-range, through-space excitonic interactions. The RR, electrochemical, and EPR data indicate that through-bond electronic communication pathways are also open in the arrays. Extremely large RR intensity enhancements are observed for aryl-ring and ethyne-bridge stretching modes. The RR intensity enhancements are attributed to an excited-state conformational change that enhances the conjugation between the π-electron systems of the porphyrin ring and bridging diarylethyne group. The half-wave potentials for oxidation of the zinc units in Zn_2, Zn_4Fb_1, and Zn_5 are slightly different. Up to four electron equivalents can be removed from Zn_2 and Zn_1Fb_1 without compromising the sample integrity; up to five electron equivalents can be removed from Zn_4Fb_1 and Zn_5. The EPR spectra of the oxidized assemblies exhibit complex temperature dependent signatures that reflect hole/electron hopping and/or spin exchange interactions. Hole/electron hopping is rapid (10^7 s^{-1} or faster) on the EPR time scale in liquid solution and slow in frozen solution. The state of the solvent rather than the temperature mediates the hopping process. Exchange interactions are significant (probably 1000 MHz or greater) in both liquid and frozen solutions and, in certain cases, are enhanced upon solvent freezing. Collectively, the studies reported provide new insights into the electronic communication pathways in the porphyrinic arrays. The studies also indicate the following: (1) The center-to-center distance of ~20 Å provided by the diarylethyne linker affords weak electronic interactions. These weak interactions facilitate rapid energy transfer but not deleterious electron-transfer quenching reactions. (2) The ability to remove five electrons from the pentameric arrays indicates their possible application as controlled-potential electron reservoirs. (3) The rapid mobility of the hole in the oxidized pentamers indicates that arrays of similar design, if fashioned in a linear architecture, could function as molecular wires or as components of electron-transport chains.

I. Introduction

Photosynthetic organisms use light-harvesting complexes to capture sunlight and funnel the energy to the reaction center.[1] Light-harvesting complexes are remarkably efficient despite the fact that energy transfer occurs over long distances and involves hundreds of chromophores.[2] Understanding the light-harvesting phenomenon at the molecular level is a long-standing objective of photosynthesis research. The elucidation of the structural and electronic properties of natural light-gathering arrays that lead to efficient energy transfer and concentration may also provide a foundation for the design of synthetic molecular devices for use in photovoltaic energy conversion/charge storage,[3] photosensitization,[4] and optical sensing.[5]

The detailed determination of the factors governing the functional characteristics of naturally occurring light-harvesting systems is difficult owing to the size and complexity of the assemblies. Consequently, synthetic porphyrin-based model systems are essential for probing the effects of molecular

[†] University of California.

[‡] Carnegie Mellon University.

[⊗] Abstract published in *Advance ACS Abstracts*, October 15, 1994.

(1) Larkum, A. W. D.; Barrett, J. *Adv. Bot. Res.* **1983**, *10*, 1-219. (b) *Photosynthetic Light-Harvesting Systems*; Scheer, H., Schneider, S., Eds.; W. deGruyter: Berlin, 1988. (c) Mauzerall, D. C.; Greenbaum, N. L. *Biochim. Biophys. Acta* **1989**, *974*, 119-140. (d) Hunter, C. N.; van Grondelle, R.; Olsen, J. D. *Trends Biochem. Sci.* **1989**, *14*, 72-76.

(2) (a) Sundstrom, V.; van Grondelle, R. In *The Chlorophylls*; Scheer, H., Ed.; CRC Press: Boca Raton, FL, 1991; pp 1097-1124. (b) Holzwarth, A. R. *Ibid.* pp 1125-1152.

(3) (a) Gregg, B. A.; Fox, M. A.; Bard, A. J. *J. Phys. Chem.* **1990**, *94*, 1586-1598. (b) Liu, C.-Y.; Pan, H.-L.; Fox, M. A.; Bard, A. J. *Science* **1993**, *261*, 897-899.

(4) (a) Pandey, R. K.; Vincente, G. H.; Shiau, F. Y.; Dougherty, T. J.; Smith, K. M.; *Proc. SPIE-Int. Soc. Opt. Eng.* **1991**, *1426*, 356-361. (b) Pandey, R. K.; Shiau, F. Y.; Meunier, I.; Ramaprasad, S.; Sumlin, A. B.; Dougherty, T. J.; Smith, K. M. *Proc. SPIE-Int. Soc. Opt. Eng.* **1992**, *1645*, 264-273. (c) Pandey, R. K.; Shiau, F. Y.; Ramachandran, R.; Dougherty, T. J.; Smith, K. M. *J. Chem. Soc., Perkin Trans. 1* **1992**, 1377-1385.

(5) (a) Anderson, H. L.; Martin, S. J.; Bradley, D. D. C. *Angew. Chem., Int. Ed. Engl.* **1994**, *33*, 655-657. (b) Anderson, H. L. *Inorg. Chem.* **1994**, *33*, 972-981.

0002-7863/94/1516-10578$04.50/0

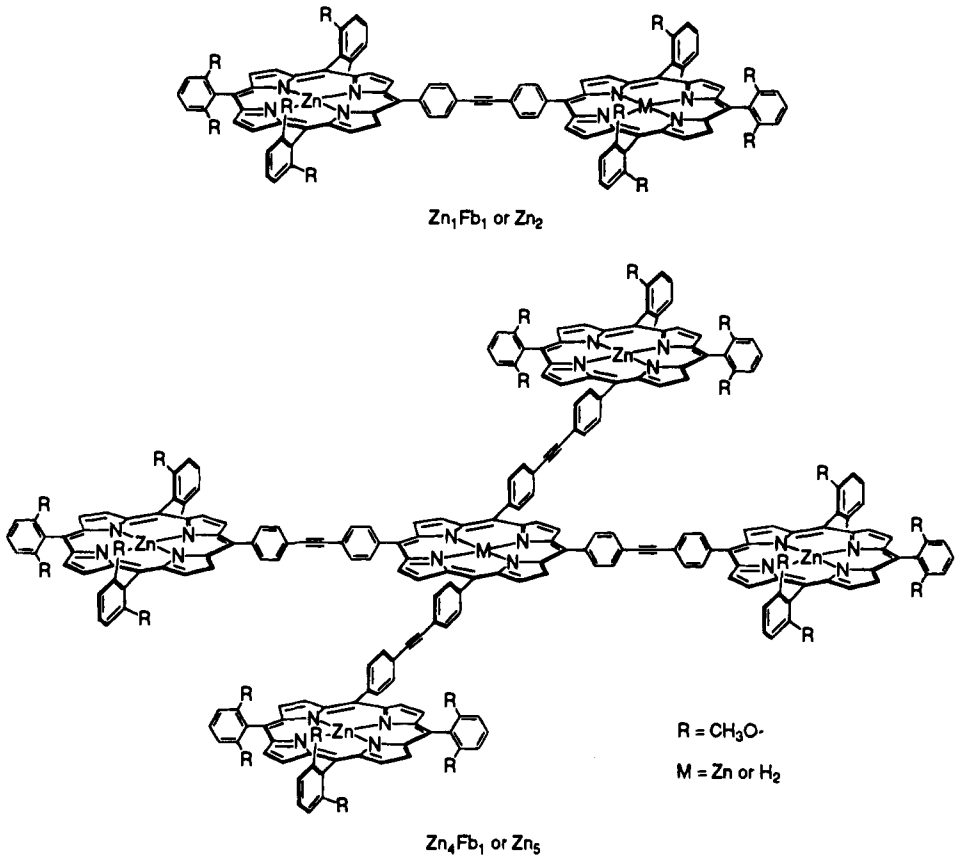

Figure 1. Structures of the dimeric and pentameric arrays.

organization on electronic communication.[5-16] Covalently linked arrays of five or more porphyrins have been prepared,[10b,g,13-15a,c] however, most of these lack the full complement of attributes necessary for a viable light-harvesting system. In addition to achieving highly efficient energy transfer, for systematic study, such systems must possess organic solubility and architectural rigidity and allow the incorporation of many porphyrinic pigments in precise states of metalation and geometrical arrangement. The scarcity of viable model light-harvesting complexes can be contrasted with the multitude of model systems that have been prepared in attempts to mimic the photoinduced, directional electron-transfer reactions that occur in photosynthetic reaction centers.[6,7]

Recently, one of our groups reported a synthetic strategy for preparing large arrays of covalently linked porphyrins which exhibit the physical and architectural properties required of a viable light-harvesting system (vide supra).[15] This strategy is based on a building block approach that links *meso*-tetraarylporphyrins via an ethyne group at the *p*-position of the aryl ring. The general architecture of the pentameric arrays is shown in Figure 1. The pentamers prepared included all free base arrays (Fb_5), all zinc complexes (Zn_5), and complexes in which the peripheral porphyrins are zinc and the central porphyrin either is a free base (Zn_4Fb_1) or contains copper (Zn_4Cu_1). The building block approach has since been extended to synthesize a number of larger arrays ranging from dimers to nonamers.[15c]

Preliminary optical studies of the pentamers suggest that the electronic interactions between the porphyrins in the array are relatively weak.[15a] The absorption spectra of these systems are approximately a superposition of the spectra of the constituent monomeric porphyrins. There is no evidence of large band splittings that would suggest substantial excitonic interactions

(6) (a) Wasielewski, M. R. In *The Chlorophylls*; Scheer, H., Ed.; CRC Press: Boca Raton, FL, 1991; pp 269–286. (b) Wasielewski, M. R. *Chem. Rev.* **1992**, *92*, 435–461.

(7) (a) Gust, D.; Moore, T. A. *Top. Curr. Chem.* **1991**, *159*, 103–151. (b) Gust, D.; Moore. T. A. *Adv. Photochem.* **1991**, *16*, 1–65. (b) Gust, D.; Moore, T. A.; Moore, A. L.; Gao, F.; Luttrull, D.; DeGraziano, J. M.; Ma, X. C.; Makings, L. R.; Lee, S.-J.; Trier, T. T.; Bittersmann, E.; Seely, G. R.; Woodward, S.; Bensasson, R. V.; Rougee, M.; DeSchryver, F. C.; Van der Auwaraer, J. *J. Am. Chem. Soc.* **1991**, *113*, 3638–3649.

(8) (a) Won, Y.; Friesner, R. A.; Johnson, M. R.; Sessler, J. L. *Photosynth. Res.* **1989**, *45*, 4767–4784. (b) Sessler, J. L.; Johnson, M. R.; Creager, S. E.; Fettinger, J. C.; Ibers, J. A. *J. Am. Chem. Soc.* **1990**, *112*, 9310–9329. (c) Sessler, J. L.; Capuano, V. L.; Harriman, A. *J. Am. Chem. Soc.* **1993**, *115*, 4618–4628.

(9) (a) Helms, A.; Heiler, D.; McLendon, G. *J. Am. Chem. Soc.* **1992**, *114*, 6227–6238. (b) Helms, A.; Heiler, D.; McLendon, G. *J. Am. Chem. Soc.* **1991**, *113*, 4325–4327. (c) McLendon, G. *Acc. Chem. Res.* **1988**, *21*, 160–167.

(10) (a) Osuka, A.; Maruyama, K. *J. Am. Chem. Soc.* **1988**, *110*, 4454–4456. (b) Osuka, A.; Maruyama, K. *J. Am. Chem. Soc.* **1990**, *112*, 3054–3059. (c) Osuka, A.; Maruyama, K.; Mataga, N.; Asahi, T.; Yamazaki, I.; Tamai, J. *J. Am. Chem. Soc.* **1990**, *112*, 4958–4959. (d) Nagata, T.; Osuka, A.; Maruyama, K. *J. Am. Chem. Soc.* **1990**, *112*, 3054–3059. (e) Osuka, A.; Nagata, T.; Maruyama, K. *Chem. Lett.* **1991**, 481–484. (f) Osuka, A.; Nagata, T.; Maruyama, K. *Chem. Lett.* **1991**, 1687–1690. (g) Osuka, A.; Liu, B.-L.; Maruyama, K. *Chem. Lett.* **1993**, 949–952.

(11) (a) Brun, A. M.; Harriman, A.; Heitz, V.; Sauvage, J.-P. *J. Am. Chem. Soc.* **1991**, *113*, 8657–8663. (b) Brun, A. M.; Atherton, S. J.; Harriman, A.; Heitz, V.; Sauvage, J.-P. *J. Am. Chem. Soc.* **1992**, *114*, 4632–4639.

(12) (a) Wasielewski, M. R.; Niemczyk, M. P.; Svec, W. A. *Tetrahedron Lett.* **1982**, *23*, 3215–3218. (b) Abdalmuhdi, I.; Chang, C. K. *J. Org. Chem.* **1985**, *50*, 411–413. (c) Seta, P.; Bienvenue, E.; Maillard, P.; Momenteau, M. *Photochem. Photobiol.* **1989**, *49*, 537–543.

(13) (a) Milgrom, L. R. *J. Chem. Soc., Perkin Trans. 1* **1983**, 2335–2339. (b) Davila, J.; Harriman, A.; Milgrom, L. R. *Chem. Phys. Lett.* **1987**, *136*, 427–430. (b) Wennerstrom, O.; Ericsson, H.; Raston, I.; Svensson, S.; Pimlott, W. *Tetrahedron Lett.* **1989**, *30*, 1129–1132.

(14) (a) Anderson, S.; Anderson, H. L.; Sanders, J. K. M. *Acc. Chem. Res.* **1993**, *26*, 469–475. (b) Anderson, H. L.; Sanders, J. K. M. *J. Chem. Soc., Chem. Commun.* **1989**, 1714–1715. (c) Anderson, S.; Anderson, H. L.; Sanders, J. K. M. *Angew. Chem., Int. Ed. Engl.* **1992**, *31*, 907–910.

(15) (a) Prathapan, S.; Johnson, T. E.; Lindsey, J. S. *J. Am. Chem. Soc.* **1993**, *115*, 7519–7520. (b) Lindsey, J. S.; Prathapan, S.; Johnson, T. E.; Wagner, R. W. *Tetrahedron* **1994**, *50*, 8941–8968. (c) Fenyo, D.; Chait, B. T.; Johnson, T. E.; Lindsey, J. S. *J. Am. Chem. Soc.*, submitted.

(16) Lin, V. S.-Y.; DiMagno, S. G.; Therien, M. J. *Science* **1994**, *264*, 1105–1111.

between the porphyrins. The weak interactions are not surprising given that the diphenylethyne linker provides a center-to-center distance of ~20 Å between the porphyrins. In contrast, highly perturbed optical spectra, indicative of very strong electronic interactions, are observed for arrays in which the porphyrins are coupled by either an ethyne or butadiyne linkage attached directly to either a β-pyrrole or *meso*-carbon atom of the tetrapyrrole macrocycle.[5,16] The fluorescent quantum yields for the Zn_5 and Fb_5 arrays are also nearly identical with those of the monomeric porphyrins (Zn_5, $\phi_f = 0.046$; Fb_5, $\phi_f = 0.12$), indicating the absence of deleterious non-energy-transfer quenching reactions. Fluorescence excitation and emission studies on Zn_4Fb_1 and Zn_4Cu_1 indicate that the energy is funneled from the peripheral zinc porphyrins to the central porphyrin such that the fluorescence quantum yield from the zinc porphyrins is reduced 12−14-fold (Zn_4Fb_1, $\phi_f = 0.0038$; Zn_4Cu_1, $\phi_f = 0.0033$).[15a] These data indicate that energy is transferred from the peripheral units to the core with greater than 90% efficiency. In the case of Zn_4Cu_1, the transferred energy is lost through nonradiative processes in the copper porphyrin. In contrast, for Zn_4Fb_1, the transferred energy is subsequently emitted by the core free base unit ($\phi_f = 0.12$) with an efficiency nearly identical to that of a monomeric free base porphyrin. This observation suggests that these types of porphyrinic arrays constructed with diarylethyne linkers might be useful as energy concentrators and/or spatially well-defined nanoscale photon sources.

The exact mechanism of energy transfer in the diarylethyne-linked porphyrin arrays has yet to be characterized in detail. A Förster-type mechanism is the most likely candidate in view of the absorption and emission characteristics of the different porphyrins and the relatively large separations between the macrocycles (center-to-center distances ~28 Å (peripheral−peripheral) and ~20 Å (peripheral−central); edge-to-edge distances ~20 Å (peripheral−peripheral) and ~13 Å (peripheral−central)).[15a] It is also possible, however, that energy transfer is to some extent mediated by direct (electron exchange) interactions through the π-electron system. The characterization of the electronic communication pathways in the diarylethyne-linked arrays requires more detailed physical and spectroscopic studies. Toward this goal, we report a comprehensive electrochemical (cyclic and square-wave voltammetry, coulometry) and static spectroscopic (absorption, resonance Raman (RR), electron paramagnetic resonance (EPR)) study of several arrays and their component parts. The spectroscopic studies were performed on singly and multiply oxidized complexes as well as the neutral species. Though the electrochemical studies were performed initially in an effort to examine electronic interactions in the arrays, our findings concerning electron mobility indicate that the pentameric arrays could serve in molecular electronic devices as constant-potential electron reservoirs or, if fashioned in a linear configuration, as electrically conducting molecular wires or as components of electron-transport chains. These electrical properties of the arrays are complementary to their photonic light-harvesting features.

The structures of the dimeric and pentameric arrays are shown in Figure 1 and include Zn_1Fb_1, Zn_2, Zn_4Fb_1, and Zn_5. During the course of the studies, the properties of several monomeric porphyrin complexes were also investigated. The structures of these complexes are shown in Figure 2 and include Zn_1s, Zn_1a, and Zn_1a'. A copper complex, Cu_1a, was also examined. The properties of the symmetrical tetraarylporphyrin monomer Zn_1s served as the benchmark for all of the electrochemical and spectroscopic studies. Collectively, these studies provide new insights into the electronic communication between the porphyrin units in the diarylethyne-linked arrays.

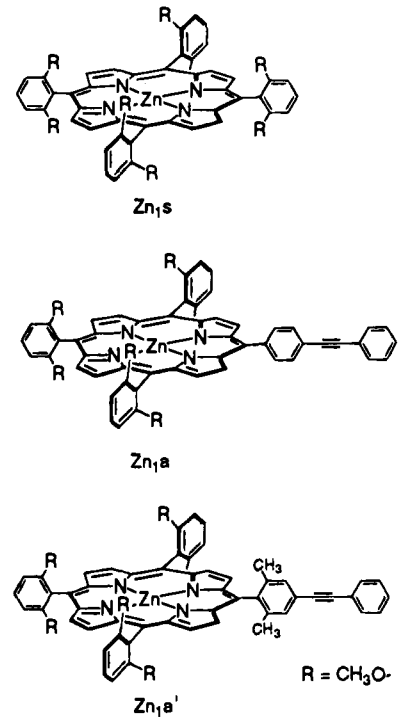

Figure 2. Structures of the monomeric porphyrins.

II. Experimental Section

The various porphyrin arrays were synthesized and characterized by methods previously described.[15] The electrochemical and spectroscopic studies were performed on samples prepared in CH_2Cl_2 or *o*-dichlorobenzene (DCB) (both from Aldrich, HPLC grade). CH_2Cl_2 was purified by vacuum distillation from P_2O_5 followed by another distillation from CaH_2; DCB was distilled from sodium. For the electrochemical studies, tetrabutylammonium hexafluorophosphate (TBAH; Aldrich, recrystallized three times from methanol and dried under vacuum at 110 °C) was used as the supporting electrolyte. The solvents were degassed thoroughly by several freeze−pump−thaw cycles prior to use.

The oxidized complexes were prepared in a glovebox (Vacuum Atmospheres HE-93 equipped with a Model 493 Dri-Train) by using standard electrochemical instrumentation (PAR 175 Universal Programmer and PAR 173 potentiostat or EG&G 263 potentiostat/galvanostat). The samples were contained in a three-compartment cell equipped with a Pt wire working electrode, a Pt mesh counter electrode, and a Ag/Ag^+ (butyronitrile) reference electrode. The oxidized species were generated by quantitative coulometry at a Pt mesh electrode. The integrity of the samples was checked by cyclic voltammetry after each successive oxidation. In all cases, the cyclic voltammograms were reproducible upon repeated scans and exhibited no scan rate dependence in the 20−100 mV/s range. Upon oxidation, the samples were transferred to an optical cuvette (absorption) or quartz capillary (RR and EPR) and carefully sealed in a glovebox. All of the spectroscopic studies on the oxidized complexes were performed immediately following the oxidation. Prior to obtaining RR and EPR spectra, absorption spectra were recorded to reconfirm the integrity of the samples.

The absorption spectra of all the neutral and oxidized complexes were obtained in the 300−800-nm range by using a diode array spectrometer (Hewlett-Packard 8254A). The sample concentration was typically 0.01 mM. The spectra of the oxidized species were also examined in the 800−3000-nm region by using a grating spectrophotometer (Cary 2390). The sample concentrations (~0.05 mM) used in the near-infrared studies were made as high as possible without inducing aggregation.

The RR spectra of the neutral and cationic species were obtained with a triple spectrograph (Spex 1877) equipped with a 2400 grooves/mm holographically etched grating in the third stage. A liquid nitrogen cooled, UV-enhanced 1152X298 pixel charge coupled device (Princeton Instruments, LN/CCD equipped with an EEV1152-UV chip) was used

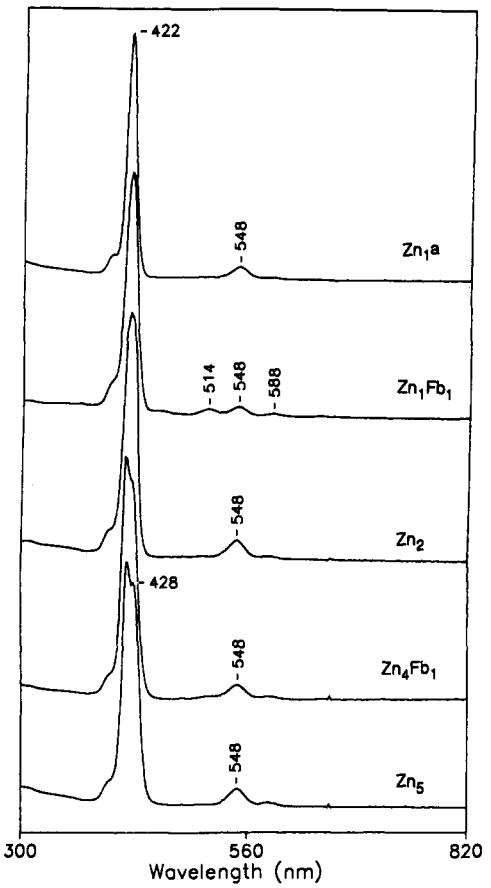

Figure 3. Absorption spectra of the neutral porphyrins in CH_2Cl_2.

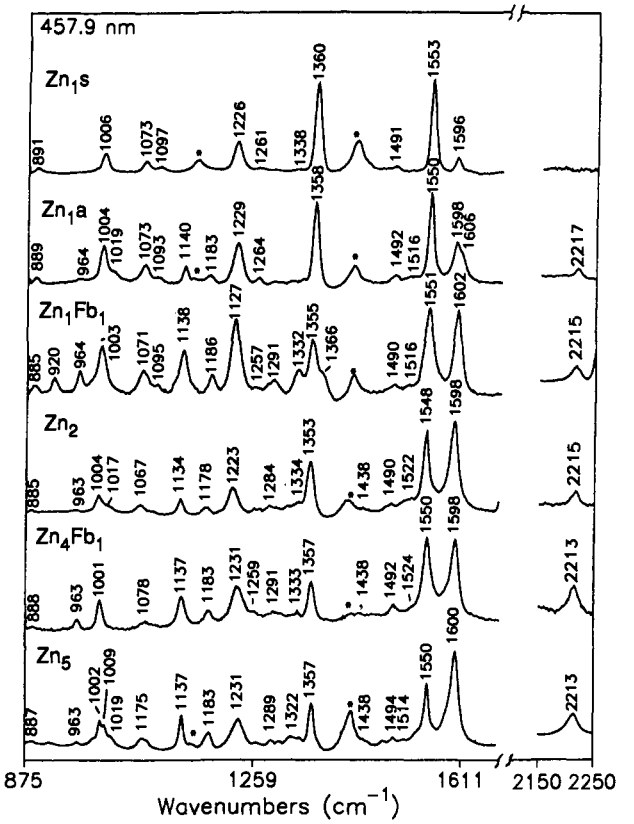

Figure 4. B-state-excitation (λ_{ex} = 457.9 nm) RR spectra of the neutral porphyrins in CH_2Cl_2. The bands marked by asterisks are due to solvent.

as the detector. The sample concentrations for the RR experiments were in the 0.05−0.5 mM range. The excitation wavelengths were provided by the outputs of either a Kr ion (Coherent Innova 200-K3) or Ar ion (Coherent Innova 400-15UV) laser. The frequencies were calibrated by using the known values of indene and CH_3CN. The frequencies are accurate to ± 1 cm^{-1} for strong and/or isolated bands. The laser power at the sample was typically less than 10 mW. The spectral resolution was ~ 2 cm^{-1} at a Raman shift of 1600 cm^{-1}.

The EPR spectra were recorded with an X-band spectrometer (Bruker ER200D) equipped with a NMR gaussmeter (Bruker ER035M) and a microwave frequency counter (Hewlett-Packard 3550B). The sample concentration was typically in the 0.04−0.05 mM range. Temperature control (100−400 K) was achieved with a continuous flow N_2 cryostat (Bruker). The microwave power and magnetic field modulation amplitude were typically 5.7 mW and 0.32 G, respectively.

III. Results

A. Neutral Complexes. (1) Absorption Spectra. The absorption spectra of the neutral arrays and a monomeric building block are shown in Figure 3. The general spectral features of all the compounds (strong B-bands and weak Q-bands) are similar to one another and similar to those of Zn_1s (not shown). The wavelengths of the B- and Q-band absorption maxima of Zn_1a are similar to those of Zn_1s, indicating that the ethyne group does not significantly perturb the π-electron system of the porphyrin ring. The absorption spectrum of the Zn_1Fb_1 is approximately a superposition of the absorption spectra of the zinc and free base porphyrin units as was previously reported for Zn_4Fb_1.[15a] The B-state absorption contours for all the dimeric and pentameric arrays are, however, slightly red-shifted relative to that of Zn_1a (or the free base of this porphyrin). The line widths for the B-bands of the arrays are also somewhat larger than that of the monomer, and in the case of Zn_4Fb_1 and Zn_5, the B-bands exhibit a small splitting (5−10 nm).[17] These effects are not manifested in the Q-state region where the absorption bands are nearly an exact superposition of the component spectra. Together, these results suggest that weak excitonic interactions occur in the B-states of the arrays.[8a,10d,e,18−21]

(2) RR Spectra. The high-frequency regions of the B-state-excitation (λ_{ex} = 457.9 nm) RR spectra of the neutral diarylethyne-linked porphyrin arrays are shown in Figure 4. The RR spectrum of Zn_1s is also included in the figure. The spectral features observed for the diarylethyne-substituted porphyrin and the arrays are similar to one another and are qualitatively similar to those of Zn_1s. These features include strong scattering from the totally symmetric modes such as ν_2 and ν_4 at $\sim$1550 and $\sim$1357 cm^{-1}, respectively.[22] No splittings are observed in any of the RR bands of the arrays that indicate significant interactions between the constituent porphyrins.[23] For Zn_1Fb_1 and Zn_4Fb_1, certain modes of the free base unit exhibit frequencies similar to those of the zinc unit(s) whereas others do not. For example, additional RR bands are observed at 1332 and 1291 cm^{-1} due to scattering by the free base units. These bands are relatively weak for Zn_4Fb_1 because the scattering from the four zinc porphyrins dominates the spectrum.

(17) In ref 15a, it is stated that the B-bands of the pentameric arrays are not split; however, a small splitting is resolved under the higher resolution conditions used to acquire the spectra reported here.

(18) Kasha, M.; Rawls, H. R.; El-Bayoumi, M. A. *Pure Appl. Chem.* **1965**, *11*, 371−392.

(19) Gouterman, M.; Holten, D.; Lieberman, E. *Chem. Phys.* **1977**, *25*, 139−153.

(20) Hunter, C. A.; Sanders, J. K. M.; Stone, A. J. *Chem. Phys.* **1989**, *133*, 395−404.

(21) Schick, G. A.; Schreiman, I. C.; Wagner, R. W.; Lindsey, J. S.; Bocian, D. F. *J. Am. Chem. Soc.* **1989**, *111*, 1344−1350.

(22) (a) Burke, J. M.; Kincaid, J. R.; Spiro, T. G. *J. Am. Chem. Soc.* **1978**, *100*, 6077−6083. (b) Burke, J. M.; Kincaid, J. R.; Peters, S.; Gagne, R. R.; Collman, J. P.; Spiro, T. G. *J. Am. Chem. Soc.* **1978**, *100*, 6083−6088. (c) Li, X.-Y.; Czernuszewicz, R. S.; Kincaid, J. R.; Su, Y. O.; Spiro, T. G. *J. Phys. Chem.* **1990**, *94*, 31−47. (d) Schick, G. A.; Bocian, D. F. *J. Am. Chem. Soc.* **1983**, *105*, 1830−1838.

(23) Adar, F.; Srivastava, T. S. *Proc. Natl. Acad. Sci. U.S.A.* **1975**, *72*, 4419−4424.

Although the RR spectra of the diarylethyne-substituted porphyrin and arrays are qualitatively similar to those of Zn_1s, there are two noteworthy differences: (1) For all of the diarylethyne-substituted porphyrins, the RR band due to the aryl ring mode, ν_{aryl},[22] at ~1600 cm^{-1} is unusually intense. In the case of Zn_1a, the intensity of this band is more than twice that of the analog band of Zn_1s. For the dimeric and pentameric arrays, the RR intensity enhancement of ν_{aryl} is extraordinarily large and is comparable to that of the strong ν_2 and ν_4 bands of the porphyrin ring. This level of RR intensity enhancement is unprecedented for an aryl ring mode of a tetraarylporphyrin. (2) For all of the diarylethyne-substituted porphyrins, a RR band is observed at ~2215 cm^{-1} which is not observed in the spectrum of Zn_1s. This band is relatively weak in the spectrum of Zn_1a but becomes moderately intense in the spectra of all the arrays. This intensity pattern parallels that observed for ν_{aryl}. Based on its frequency, we assign the 2215-cm^{-1} RR band as the stretching vibration of the ethyne group, $\nu_{C\equiv C}$. The fact that this mode exhibits any degree of resonance enhancement is surprising considering that this group is five bonds away from the porphyrin π-system.

In order to gain further insight into the factors influencing the RR enhancements of ν_{aryl} and $\nu_{C\equiv C}$, several other studies were performed. First, the RR spectra of Zn_1a were obtained at a variety of excitation wavelengths in the B-state region. These studies showed that the relative intensities of ν_{aryl} and $\nu_{C\equiv C}$ vary significantly with respect to those of the porphyrin modes as the excitation wavelength is changed. The studies on Zn_1a could not be extended to the Q-state region because of the strong fluorescence from the complex. Therefore, additional studies were performed on Cu_1a. This complex does not fluoresce, which permits the acquisition of Q-state-excitation RR spectra.

The high-frequency regions of the RR spectra of Cu_1a obtained with various excitation wavelengths spanning the B- and Q-state regions are shown in Figure 5. The absolute RR intensities observed at the different excitation wavelengths cannot be directly compared because the sample concentrations required to obtain reasonable quality Q-state spectra are higher than those necessary for B-state studies. The data do, however, provide a means for comparing the RR intensities of the porphyrin modes relative to those of ν_{aryl} (~1600 cm^{-1}) and $\nu_{C\equiv C}$ (~2215 cm^{-1}) at a given excitation wavelength. With excitation in the B-state region, the RR intensity enhancement patterns observed for Cu_1a are essentially identical to those of Zn_1a. In particular, the RR intensities of ν_{aryl} and $\nu_{C\equiv C}$ decrease relative to those of the porphyrin modes as the excitation wavelength is tuned past the B-band absorption maximum toward the B-state vibronic satellites. With λ_{ex} = 413.1 nm, ν_{aryl} is very weak and $\nu_{C\equiv C}$ is not observed at all. In contrast, the intensities of these modes increase significantly as the excitation wavelength is tuned toward the Q-bands. In general, the intensities of ν_{aryl} and $\nu_{C\equiv C}$ appear to track one another. The largest intensities occur when the excitation wavelength falls in the 450−500-nm region. The absorption features in this spectral region are very weak (Figure 1) and correspond to high vibronic satellites of the Q-state.[24] For comparison, the RR enhancements of ν_{aryl} of Zn_1s were also investigated (not shown). These studies indicate that ν_{aryl} of the symmetrical porphyrin also exhibits the largest intensity with excitation in the 450−500-nm region.

In another series of studies, RR spectra were obtained for a derivative of Zn_1a in which the *o*-hydrogens of the aryl ring containing the *p*-ethyne group were replaced by methyl groups

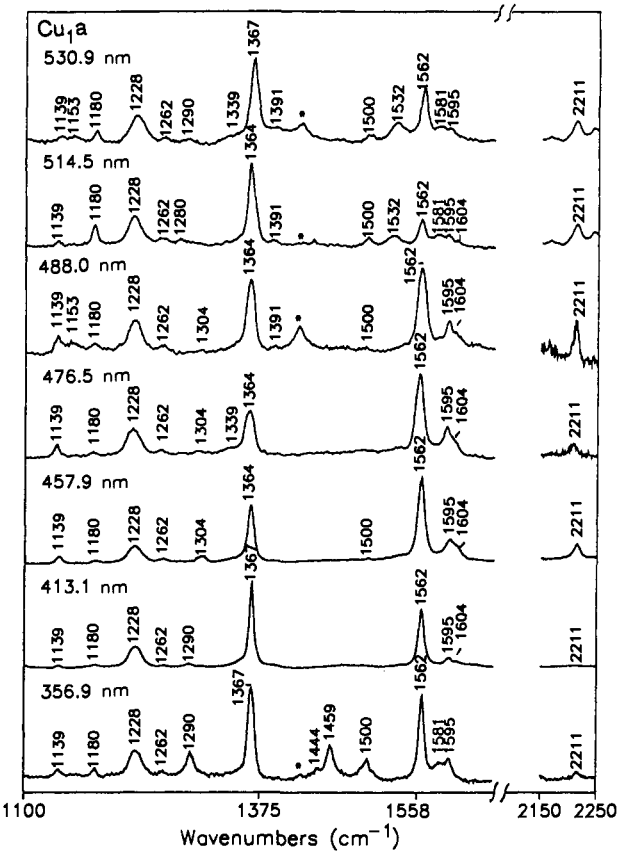

Figure 5. RR spectra of Cu_1a in CH_2Cl_2 at different excitation wavelengths. The bands marked by asterisks are due to solvent.

(Zn_1a'). The introduction of the *o*-methyl substituents increases the steric interactions between the aryl group and the porphyrin macrocycle. These interactions should constrain the aryl and porphyrin rings to a more non-coplanar conformation (Scheme 1). The introduction of the *o*-dimethyl substituents does not significantly alter the absorption spectrum from that observed for Zn_1a. The shifts in the absorption bands are at most 1−2 nm (not shown). In contrast, the RR spectra of the two complexes are quite different. This is illustrated in Figure 6, which compares the RR spectra obtained with λ_{ex} = 457.9 nm. The intensity of the ν_{aryl} band (~1600 cm^{-1}) of Zn_1a' is significantly less than that observed for Zn_1a (although it is still greater than that observed for Zn_1s, cf. Figure 4). In addition, no band attributable to $\nu_{C\equiv C}$ (~2215 cm^{-1}) is observed in the RR spectrum of Zn_1a'. These results indicate that the electronic interactions between the porphyrin and ethynylphenyl rings are significantly reduced when *o*-dimethyl groups impede rotation about the *meso*-aryl C−C bond.

B. Oxidized Complexes. (1) Electrochemistry. The $E_{1/2}$ values for oxidation of the various zinc complexes in CH_2Cl_2 are summarized in Table 1. The two $E_{1/2}$ values listed in the table correspond to the first and second oxidations of the porphyrin ring.[25] The redox potentials observed for Zn_1a are nearly identical to those obtained for Zn_1s, reflecting minimal perturbation of the porphyrin π-system by the ethyne group. The $E_{1/2}$ value for oxidation of diphenylethyne is 1.64 V vs SCE[26] and its absorption λ_{max} occurs at ~300 nm,[27] indicating that the highest occupied and lowest unoccupied molecular

(24) Gouterman, M. In *The Porphyrins*; Dolphin, D., Ed.; Academic Press: New York, 1978; Vol. III, pp 1−165.

(25) (a) Felton, R. H. In *The Porphyrins*; Dolphin, D., Ed.; Academic Press: New York, 1978; Vol. V, pp 53−126. (b) Davis, D. G. *Ibid.* pp 127−152.

(26) Cariou, M.; Simonet, J. *J. Chem. Soc., Chem. Commun.* **1990**, 445−446.

(27) Armitage, J. B.; Entwistle, N.; Jones, E. R. H.; Whiting, M. C. *J. Chem. Soc.* **1954**, 147−154.

Scheme 1. Hindered Torsional Motion about the *meso*-Aryl C–C Bond of the *o*-Dimethylaryl Unit of Zn_1a'

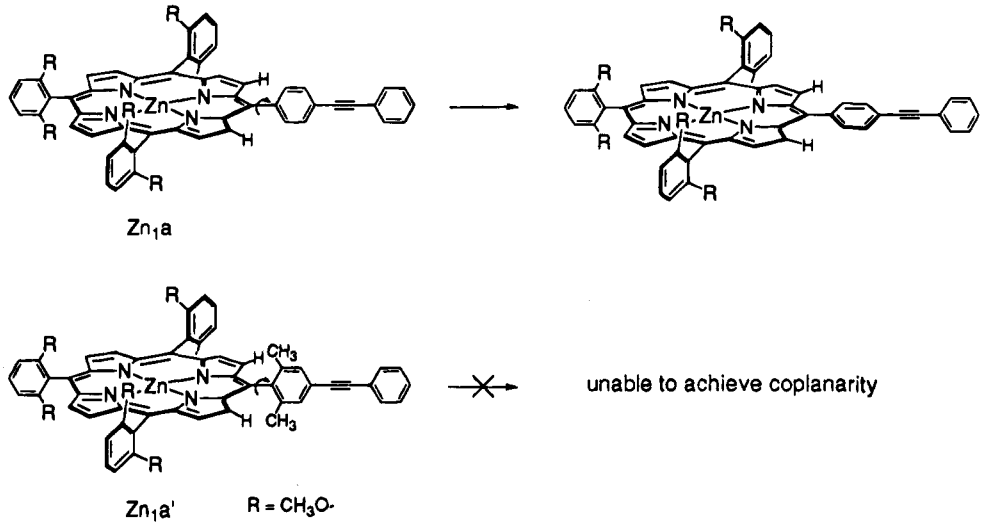

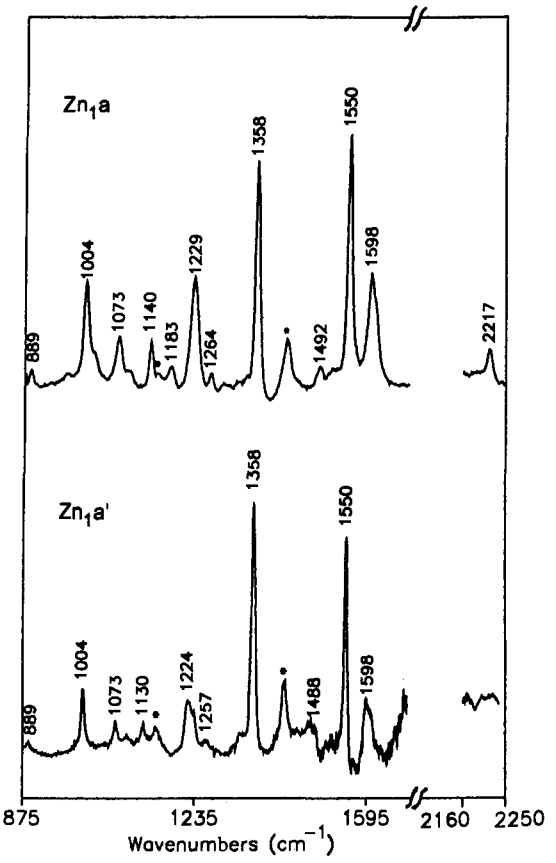

Figure 6. B-state-excitation (λ_{ex} = 457.9 nm) RR spectra of Zn_1a and Zn_1a' in CH_2Cl_2. The bands marked by asterisks are due to solvent.

orbitals of diphenylethyne span those of the porphyrin. In the case of Zn_1Fb_1, four overlapping redox waves are observed, two each for the zinc and free base porphyrins. The $E_{1/2}$ values for oxidation of the zinc and free base units of the array are similar to those of monomeric zinc and free base porphyrins.[25] In the case of Zn_2, two redox waves are observed at ~0.55 and ~0.85 V. These two $E_{1/2}$ values are similar to those of the first and second porphyrin ring oxidations of Zn_1a. The anodic to cathodic peak-to-peak separation for each of these waves observed for Zn_2 is ~70 mV, suggesting that each wave corresponds to two one-electron redox processes. Quantitative coulometry confirms that each wave corresponds to the removal of two electrons. These studies, in conjunction with cyclic voltammetry, indicate that up to four electron equivalents can be removed from Zn_2 (and Zn_1Fb_1) without seriously compromising its integrity. Differential pulse and square-wave voltammetry on Zn_2 failed to resolve peaks due to the individual one-electron oxidations; however, each of the peaks exhibits a discernible asymmetry that is not observed for Zn_1a. This result suggests that the $E_{1/2}$ values for the unresolved one-electron oxidations of Zn_2 are similar although not identical (within 50 mV). These results are consistent with the absorption characteristics of the complex which are indicative of weak interactions between the porphyrin units. Preliminary electrochemical studies on dimeric arrays in which the 2,6-dimethoxyphenyl groups are replaced by mesityl groups reveal that the general redox behavior is identical to that described above (although the $E_{1/2}$ values are shifted). These results indicate that the trends observed in the redox behavior are not sensitive to the nature of the nonbridging *meso*-aryl groups.

Table 1. Half-Wave Potentials[a] for Oxidation of the Porphyrin Rings of the Various Complexes

	zinc porphyrin		free base porphyrin	
	$E_{1/2}$ (1)	$E_{1/2}$ (2)	$E_{1/2}$ (1)	$E_{1/2}$ (2)
Zn_1s	0.56	0.85		
Zn_1a	0.56	0.85		
Zn_1Fb_1[b]	0.54	0.81	0.65	1.06
Zn_2	0.55[c]	0.84[c]		
Zn_4Fb_1	0.56[c]	0.86[c]	*d*	1.04[e]
Zn_5	0.54[c,f]	0.84[c]		
	0.66[g]			

[a] Obtained in CH_2Cl_2 containing 0.1 M TBAH. $E_{1/2}$ vs Ag/Ag^+; $E_{1/2}$ of $FeCp_2/FeCp_2^+$ = 0.22 V; scan rate = 0.1 V/s. Values are ±0.01 V. [b] Values are approximate due to the overlap of zinc and free base waves. [c] The redox waves due to different zinc porphyrin units are not resolved by the cyclic voltammetry. Consequently, only two waves corresponding to the first and second ring oxidations are observed.[d] This wave is obscured by the broad zinc $E_{1/2}$ (1) waves. [e] Value obtained from square-wave voltammetry. [f] Peripheral porphyrins. [g] Central porphyrin.

Zn_4Fb_1 exhibits redox waves at ~0.56, ~0.86, and ~1.04 V. The $E_{1/2}$ values for the first two waves are similar to those observed for the first and second oxidations of Zn_1a. Quantitative coulometry of Zn_4Fb_1 indicates that the lowest potential peak is due to the four overlapped one-electron oxidations of the zinc units. Square-wave voltammetry shows that this peak is asymmetrical. Part of this asymmetry is due to small differences in the $E_{1/2}$ values of the overlapping one-electron oxidations of the four zinc units. The remainder of the asymmetry is most likely due to the presence of a peak from the first oxidation of the free base unit. The $E_{1/2}$ value for this latter oxidation should fall between the values for the first and second oxidations of the zinc porphyrins. The wave observed

for Zn_4Fb_1 at ~0.86 V is assigned to the latter oxidation on the basis of its $E_{1/2}$ value (Table 1). The presence of an underlying wave due to the first oxidation of the free base unit of Zn_4Fb_1 is further supported by quantitative coulometry which indicates that a fifth electron can be removed from the complex when the potential is poised at ~0.78 V. The quantitative coulometric studies also indicate that only five electrons can be reversibly removed from Zn_4Fb_1. Removal of a sixth electron results in significant sample degradation. The wave observed for Zn_4Fb_1 at ~1.04 V is attributed to the second oxidation of the free base unit on the basis of its $E_{1/2}$ value.

Zn_5 exhibits two major redox waves at ~0.54 and ~0.86 V and a third weaker wave at ~0.66 V. The $E_{1/2}$ values for the lowest and highest potential waves are similar to those of the first and the second oxidations of Zn_1a. Quantitative coulometry confirms that the lowest potential wave corresponds to four one-electron oxidations. The wave observed at ~0.66 V by cyclic voltammetry is clearly resolved by differential pulse and square-wave voltammetry. The integrated area of the weak feature is approximately one-quarter of each of the two main redox peaks for Zn_5. This observation suggests that the weak feature observed at ~0.66 V may be due to the first oxidation of the central zinc unit. Quantitative coulometry shows that an additional electron can be removed from Zn_5 when the potential is poised at ~0.78 V. The quantitative coulometric studies also indicate that only five electrons can be removed from Zn_5 before appreciable sample decomposition occurs. The wave due to the second oxidation of the core porphyrin could not be identified. This wave would be expected at a slightly higher potential than that observed for the analogous wave(s) of the peripheral porphyrins (~0.86 V).

Results obtained in the EPR studies on the oxidized dimeric and pentameric arrays (vide infra) prompted us to investigate their electrochemical properties in solvents other than CH_2Cl_2. The principal criterion for these studies was that the solvents have a substantially different freezing point than that of CH_2Cl_2. The solvents which best meet this and three other criteria needed for the studies (electrochemistry compatibility, stability of the porphyrin cation radicals,[28] and array solubility) are halogenated benzenes such as DCB. The electrochemistry of all the complexes in DCB is similar to that observed in CH_2Cl_2 except that the first and second oxidation potentials shift cathodically by ~200 and ~20 mV, respectively.

(2) Absorption Spectra. The UV−vis absorption spectra of Zn_1a, Zn_1Fb_1, Zn_2, and their oxidation products in CH_2Cl_2 are shown in Figure 7. The spectra of the neutral and cationic complexes of Zn_4Fb_1 and Zn_5 are compared in Figure 8. The spectral characteristics of all of the oxidized complexes are similar to one another and typical of other porphyrin π-cation radicals, namely weaker, blue-shifted B-bands and very weak, broad bands in the visible and near-infrared regions.[25a] The absorption spectra of the oxidized complexes appear to be a superposition of the spectra of the neutral and cationic species of the different porphyrin units. This observation is consistent with the weak interactions[29-32] between the constituent zinc porphyrins indicated by the electrochemical studies. Despite the weakness of these interactions, the near-infrared absorption spectrum of $[Zn_2]^+$ was carefully examined (not shown) in order to search for bands indicative of intervalence charge-transfer

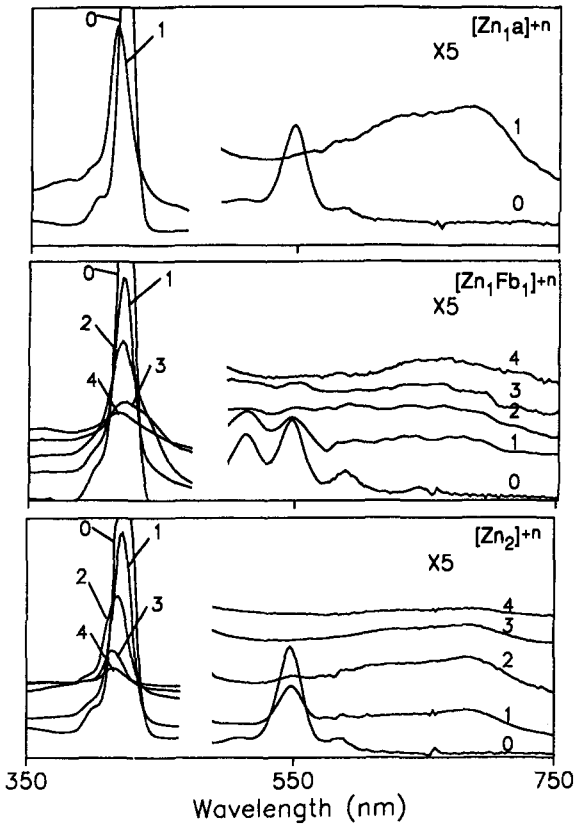

Figure 7. Absorption spectra of $[Zn_1a]^+$, $[Zn_1Fb_1]^{+n}$, and $[Zn_2]^{+n}$ in CH_2Cl_2 ($n = 0-4$). The number on each spectrum represents the value of n. The spectra in the 500−750-nm range are scaled by a factor of 5 and offset to facilitate comparison.

transitions.[33] However, no evidence could be found for such transitions; the spectrum of $[Zn_2]^+$ in the 800−3000-nm range is essentially identical to that of $[Zn_1a]^+$.

The similar $E_{1/2}$ values observed for the one-electron oxidations of the zinc units in Zn_2, Zn_4Fb_1, and Zn_5 raise the possibility that the oxidation products could disproportionate into mixtures in which a variety of oxidation states coexist.[34] In the case of Zn_2, only the mono- and trications can disproportionate (to yield Zn_2 and $[Zn_2]^{+2}$ or $[Zn_2]^{+2}$ and $[Zn_2]^{+4}$, respectively). In the case of the pentameric arrays, the disproportionation pattern could be much more complicated. It is not possible to determine from the absorption spectra alone whether disproportionation occurs because there are no spectral signatures that distinguish between the various oxidation states of complexes. Indeed, simulations of the B-state absorption of $[Zn_2]^+$ indicate that the observed features could also be accounted for by a 50/50 mixture of the spectra observed for Zn_2 and $[Zn_2]^{+2}$. Regardless, the RR and EPR studies on the arrays show that each of the oxidized species exhibits unique spectral features, indicating that no appreciable disproportionation occurs (vide infra).

(3) RR Spectra. The high-frequency regions of the B-state-excitation (λ_{ex} = 457.9 nm) RR spectra of Zn_1a, $[Zn_1a]^+$, Zn_2, $[Zn_2]^+$, and $[Zn_2]^{+2}$ are shown in Figure 9. The RR spectra of

(28) Shine, H. J.; Padilla, G. A.; Wu, S.-M. *J. Org. Chem.* **1979**, *44*, 4069−4075.

(29) Heath, G. A.; Yellowlees, L. J.; Braterman, P. S. *J. Chem. Soc., Chem. Commun.* **1981**, 287−289.

(30) Elliot, C. M.; Hershenhart, E. *J. Am. Chem. Soc.* **1982**, *104*, 7519−7526.

(31) Edwards, W. D.; Zerner, M. C. *Can. J. Chem.* **1985**, *63*, 1763−1772.

(32) (a) Angel, S. M.; DeArmond, M. K.; Donohoe, R. J.; Wertz, D. W. *J. Phys. Chem.* **1985**, *89*, 282−285. (b) Donohoe, R. J.; Tait, C. D.; DeArmond, M. K.; Wertz, D. W. *Spectrochim. Acta* **1986**, *42A*, 233−240. (c) Tait, C. D.; Macqueen, D. B.; Donohoe, R. J.; DeArmond, M. K.; Hanck, K. W.; Wertz, D. W. *J. Phys. Chem.* **1986**, *90*, 1766−1771. (d) Donohoe, R. R.; Tait, C. D.; DeArmond, M. K.; Wertz, D. W. *J. Phys. Chem.* **1986**, *90*, 3923−3926. (e) Donohoe, R. J.; Tait, C. D.; DeArmond, M. K.; Wertz, D. W. *J. Phys. Chem.* **1986**, *90*, 3927−3930.

(33) Robin, M. B.; Day, P. *Adv. Inorg. Chem. Radiochem.* **1967**, *10*, 247−422.

(34) Chen, C. H.; Doney, J. J.; Reynolds, G. A.; Saeva, F. D. *J. Org. Chem.* **1983**, *48*, 2757−2761.

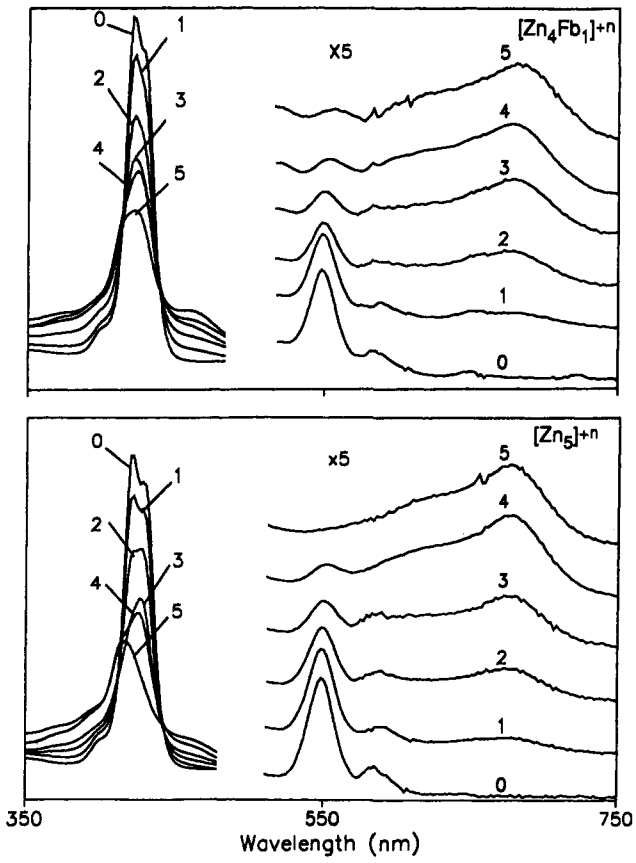

Figure 8. Absorption spectra of $[Zn_4Fb_1]^{+n}$ and $[Zn_5]^{+n}$ in CH_2Cl_2 (n = 0–5). The number on each spectrum represents the value of n. The spectra in the 500–750-nm range are scaled by a factor of 5 and offset to facilitate comparison.

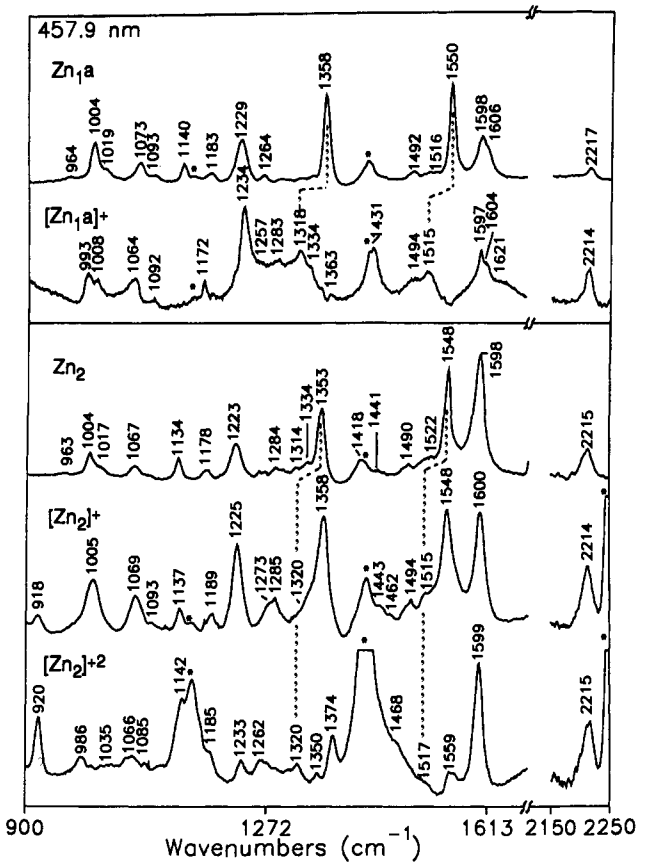

Figure 9. B-state-excitation (λ_{ex} = 457.9 nm) RR spectra of Zn_1a, $[Zn_1a]^+$, Zn_2, $[Zn_2]^+$, and $[Zn_2]^{+2}$ in CH_2Cl_2. The bands marked by asterisks are due to solvent.

the oxidation products of Zn_1Fb_1, Zn_4Fb_1, and Zn_5 were not obtained. The oxidation-induced spectral changes observed for all the diarylethyne-substituted porphyrins and arrays are similar to one another and similar to those observed for other tetraarylporphyrins.[35] The most pronounced effect is the large downshift exhibited by both ν_2 and ν_4. In the case of $[Zn_1a]^+$, oxidation downshifts these modes from 1550 to 1515 cm^{-1} and from 1358 to 1318 cm^{-1}, respectively. These large RR frequency shifts are typical of $^2A_{2u}$ cation radicals.[35] Oxidation also results in a general decrease in the RR scattering cross section of the porphyrin modes. In contrast, ν_{aryl} and $\nu_{C\equiv C}$ are more intense (relative to the porphyrin modes) in the oxidized complex than in the neutrals. However, the frequencies of these modes are not affected by oxidation.

Inspection of Figure 9 reveals that the RR spectra of $[Zn_2]^+$ are distinctly different from those of either $[Zn_1a]^+$ or $[Zn_2]^{+2}$. In particular, $[Zn_2]^+$ exhibits features common to both neutral and cationic complexes, whereas only cation features are observed for either $[Zn_1a]^+$ or $[Zn_2]^{+2}$. For example, the RR spectrum of $[Zn_2]^+$ contains strong bands attributable to ν_2 and ν_4 of a neutral at 1556 and 1358 cm^{-1}, respectively, and weak features due to these modes of a cation at 1515 and 1320 cm^{-1}. These spectral features are most consistent with one neutral and one oxidized zinc porphyrin in a single dimeric array rather than with a mixture of Zn_2 and $[Zn_2]^{+2}$ (formed by disproportionation). This is exemplified by the fact that the ν_4 band of the "neutral half" of $[Zn_2]^+$ is upshifted by 5 cm^{-1} compared with that of the analogous band of Zn_2. In addition, the relative intensities of a number of the RR bands of $[Zn_2]^+$, for example, those at 1005, 1069, and 1225 cm^{-1}, cannot be accounted for by adding the spectra of Zn_2 and $[Zn_2]^{+2}$ in any proportions.

(35) Czernuszewicz, R. S.; Macor, K. A.; Li, X.-Y.; Kincaid, J. R.; Spiro, T. G. *J. Am. Chem. Soc.* **1989**, *111*, 3860–3869.

(4) EPR Spectra. The EPR spectra of the oxidation products of Zn_1a, Zn_1Fb_1, and Zn_2 in CH_2Cl_2 at 295 and 100 K are shown in Figure 10. The temperature dependence of the nuclear hyperfine splittings or peak-to-peak line widths (when hyperfine structure is not observed) are reported in Table 2. The EPR spectra of all of the cations were examined as a function of sample concentration. No changes in hyperfine splittings or line shape were observed in the concentration range used for the EPR studies. Consequently, the differences observed in the spectral features of the various complexes are intrinsic and cannot be ascribed to intermolecular interactions. Preliminary EPR studies on dimeric arrays in which the 2,6-dimethoxyphenyl groups are replaced by mesityl groups reveal that the spectra are identical to those shown in Figure 10. These results indicate that the spectral characteristics are not sensitive to the nature of the nonbridging *meso*-aryl groups.

In the case of $[Zn_1a]^+$, a nine-line hyperfine pattern is observed in liquid solution due to interaction of the unpaired electron with the four pyrrolic ^{14}N nuclei ($a^{14}_N \sim 1.6$ G (4.5 MHz)). This spectral pattern is characteristic of a $^2A_{2u}$ porphyrin π-cation radical.[36] The general spectral features and hyperfine splittings observed for $[Zn_1a]^+$ are essentially identical to those of $[Zn_1s]^+$ (not shown). This observation indicates that the addition of the ethyne group does not significantly alter the spin-density distribution in the porphyrin. In frozen solution, no hyperfine structure is resolved for either $[Zn_1a]^+$ or $[Zn_1s]^+$; however, the peak-to-peak line width of the unresolved signal (~5.7 G) is similar to the full width of the structured signal observed at room temperature.

The liquid and frozen solution EPR spectra of $[Zn_1Fb_1]^+$ are very similar to those of $[Zn_1a]^+$. There is no discernible

(36) Fajer, J.; Davis, M. S. In *The Porphyrins*; Dolphin, D., Ed.; Academic Press: New York, 1979; Vol. IV, pp 197–256.

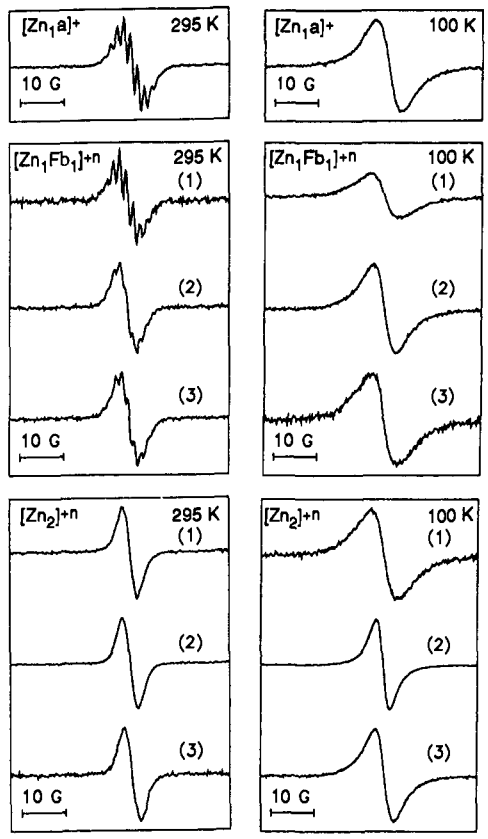

Figure 10. EPR spectra of $[Zn_1a]^+$, $[Zn_1Fb_1]^{+n}$, and $[Zn_2]^{+n}$ in CH_2Cl_2 at 295 and 100 K ($n = 1-3$). The number on each spectrum represents the value of n.

Table 2. Temperature Dependence of the Peak-to-Peak EPR Line Widths or Hyperfine Splittings (in Parentheses) for the Zn_1a and one-, two-, and three-Electron Oxidation Products of Zn_1Fb_1 and Zn_2 in CH_2Cl_2[a]

		Zn_1Fb_1			Zn_2		
T (K)	Zn_1a	1	2	3	1	2	3
100	5.7	5.7	4.9	5.5	5.7	3.1	5.5
130	5.7	5.7	4.9	5.5	5.7	3.1	5.5
160	5.7	5.7	4.9	5.5	5.7	3.1	5.5
180	(1.6)	(1.6)	(1.6)	(1.5)	(1.4)	3.9	(1.4)
210	(1.6)	(1.6)	(1.6)	(1.5)	(1.4)	3.7	(1.4)
240	(1.6)	(1.6)	(1.6)	(1.5)	(1.4)	3.5	(1.4)
270	(1.6)	(1.6)	(1.6)	(1.5)	3.5	3.5	3.5
295	(1.6)	(1.6)	(1.6)	(1.5)	3.5	3.5	3.5

[a] Line widths and hyperfine splittings (G) are ±0.1 G.

difference in the magnitude of the hyperfine splittings or the line widths for the two compounds. This observation indicates that the hole in the dimer resides exclusively on the zinc porphyrin, as expected on basis of the relative oxidation potentials of the zinc and free base units (Table 1). The liquid and frozen solution EPR spectra of $[Zn_1Fb_1]^{+2}$ are qualitatively similar to those of $[Zn_1Fb_1]^+$. There is no evidence for triplet signals in either the $g = 2$ or $g = 4$ regions.[37] This observation indicates that the dipole–dipole and exchange interactions in the biradical are relatively weak. Regardless, there are some differences in the EPR signatures of $[Zn_1Fb_1]^+$ and $[Zn_1Fb_1]^{+2}$. First, the hyperfine splittings for $[Zn_1Fb_1]^{+2}$ in liquid solution are not as well resolved as those of $[Zn_1Fb_1]^+$ and the full width of the band contour of the former complex (~4.2 G) is less than that of the latter (~5.7 G). This loss of resolution is probably due to the fact that the zinc and free base units of the biradical have slightly different hyperfine couplings. However, this does not explain the reduction in line width. Second, the line width observed for $[Zn_1Fb_1]^{+2}$ is temperature dependent and increases to ~5.0 G in frozen solution. In contrast, the width of the band contour observed for $[Zn_1Fb_1]^+$ is temperature independent. Formation of $[Zn_1Fb_1]^{+3}$ partially restores the spectral features characteristic of $[Zn_1Fb_1]^+$. In particular, the hyperfine structure observed for $[Zn_1Fb_1]^{+3}$ at room temperature is better resolved than that observed for $[Zn_1Fb_1]^{+2}$ (although not as well resolved as that for $[Zn_1Fb_1]^+$). This can be attributed to the fact that the signal for $[Zn_1Fb_1]^{+3}$ arises from a single species (the free base cation) rather than to a superposition of signals from two different species. In frozen solution, the line width observed for $[Zn_1Fb_1]^{+3}$ (~5.5 G) is somewhat larger than that observed for $[Zn_1Fb_1]^{+2}$ (~5.0 G) and is comparable to that exhibited by $[Zn_1Fb_1]^+$ (~5.7 G).

The liquid solution EPR spectrum of $[Zn_2]^+$ is distinctly different from that of $[Zn_1Fb_1]^+$ or $[Zn_1a]^+$. No hyperfine structure is resolved for $[Zn_2]^+$, and the peak-to-peak line width of the unstructured signal is significantly less than that of the full width of the structured signal observed for the latter complexes (~3.5 versus ~5.7 G). As the temperature is lowered, the EPR signal for $[Zn_2]^+$ broadens slightly. Near the freezing point of the solvent, hyperfine structure appears. The magnitude of the hyperfine splitting observed for $[Zn_2]^+$ at these temperatures is comparable to that observed for $[Zn_1Fb_1]^+$ and $[Zn_1a]^+$. When the solvent freezes, the signal for $[Zn_2]^+$ broadens and the hyperfine structure is lost. Below the freezing point of the solvent, the line width of the EPR signal for $[Zn_2]^+$ is independent of temperature and similar to that observed for $[Zn_1Fb_1]^+$ and $[Zn_1a]^+$ (~5.7 G).

The liquid solution EPR spectra of $[Zn_2]^{+2}$ and $[Zn_2]^{+3}$ are similar to that of $[Zn_2]^+$ in that their signals are narrow (~3.5 G) and no hyperfine structure is resolved. In the case of $[Zn_2]^{+2}$, there is no evidence for EPR signals characteristic of a triplet state.[37] This observation indicates that the spin–spin interactions in this biradical are weak as is also the case for $[Zn_1Fb_1]^{+2}$. Despite the similarities in the liquid solution EPR spectra of $[Zn_2]^{+2}$ and $[Zn_2]^{+3}$, the temperature dependence of their signals and their frozen solution spectra are different. The behavior observed for $[Zn_2]^{+3}$ parallels that observed for $[Zn_2]^+$. In particular, the EPR signal broadens slightly as the temperature is lowered and exhibits well-resolved hyperfine structure near the freezing point of the solvent. This structure is lost upon solvent freezing. The line width observed for $[Zn_2]^{+3}$ in frozen solution (~5.5 G) is larger than that observed in liquid solution (~3.5 G) and nearly identical to that observed for $[Zn_2]^+$ in frozen solution (~5.7 G). In the case of $[Zn_2]^{+2}$, the EPR signal also broadens slightly near the freezing point of the solvent; however, no hyperfine structure is observed. Upon solvent freezing, the EPR signal for $[Zn_2]^{+2}$ narrows rather than broadens. The frozen solution line width (~3.1 G) is less than that observed at room temperature (~3.5 G). These observations suggest that the same processes modulate the EPR signatures of $[Zn_2]^{+3}$ and $[Zn_2]^+$ and that these processes are different from those that govern the spectral characteristics of $[Zn_2]^{+2}$.

The EPR spectra of the oxidation products of Zn_4Fb_1 and Zn_5 in CH_2Cl_2 at 295 and 100 K are shown in Figure 11. The temperature dependences of the peak-to-peak line widths of the EPR signals are listed in Table 3. The EPR spectra of the oxidized pentameric arrays were examined as a function of sample concentration and found to be independent of concentration in the range used for the experiments. Consequently, the

(37) (a) Wertz, J. E.; Bolton, J. R. *Electron Spin Resonance: Elementary Theory and Practical Applications*; McGraw-Hill: New York, 1972; pp 223–257. (b) Carrington, A.; McLachlan, A. D. *Introduction to Magnetic Resonance*; Harper and Row: New York, 1967; pp 115–131.

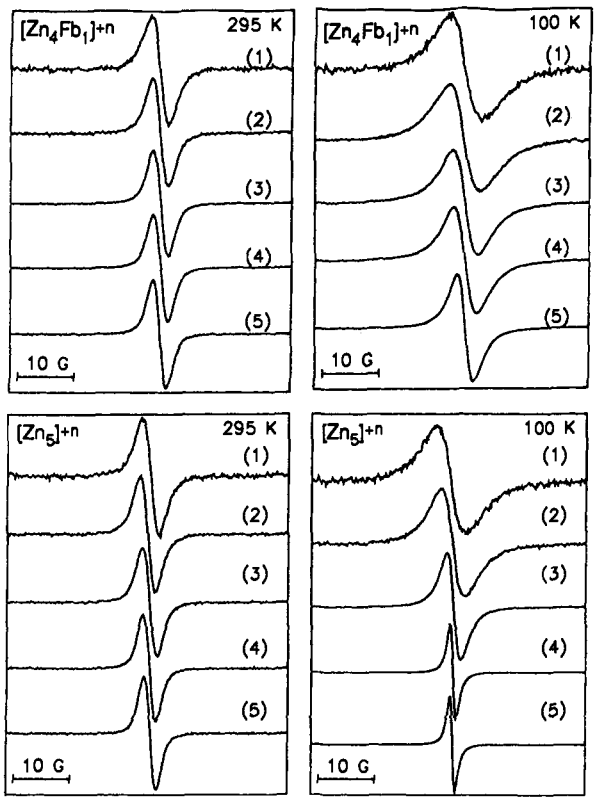

Figure 11. EPR spectra of $[Zn_4Fb_1]^{+n}$ and $[Zn_5]^{+n}$ in CH_2Cl_2 at 295 and 100 K ($n = 1-5$). The number on each spectrum represents the value of n.

Table 3. Temperature Dependence of the Peak-to-Peak EPR Line Widths for the one-, two-, three-, four-, and five-Electron Oxidation Products of Zn_4Fb_1 and Zn_5 in CH_2Cl_2[a]

	Zn_4Fb_1					Zn_5				
T (K)	1	2	3	4	5	1	2	3	4	5
100	5.7	5.5	4.7	4.5	3.1	5.7	4.3	2.7	1.2	1.0
130	5.7	5.5	4.7	4.5	2.9	5.7	4.3	2.5	1.2	1.0
160	5.7	5.5	4.7	4.5	2.9	5.7	4.3	2.3	1.0	1.0
180	3.7	3.5	3.3	3.3	3.3	3.5	3.1	3.1	2.5	2.5
210	3.5	3.3	3.1	3.1	3.1	3.5	3.1	3.1	2.5	2.5
240	2.9	2.9	2.5	2.9	2.9	2.9	2.9	2.7	2.5	2.5
270	2.9	2.9	2.7	2.7	2.7	2.9	2.9	2.5	2.3	2.3
295	2.9	2.9	2.7	2.5	2.5	2.9	2.5	2.5	2.3	2.3

[a] Line widths (G) are ±0.1 G.

different spectral features exhibited by the various complexes are intrinsic and cannot be ascribed to intermolecular interactions.

The liquid solution EPR spectra of all the cations of the pentameric arrays are similar to one another and are characterized by narrow lines with no resolved hyperfine structure. The line widths for these signals (2.3−2.9 G) are less than those observed for the cations of Zn_2 (~3.5 G). As is the case for $[Zn_2]^{+2}$ and $[Zn_1Fb_1]^{+2}$, the EPR spectra of the multiply oxidized pentameric arrays show no evidence of significant spin−spin coupling (triplet or multiplet structure). The temperature dependence of the EPR signatures of the cations of the pentameric arrays depends on the oxidation state of the complex. These temperature dependent features are described in more detail below.

The temperature dependences observed for the EPR signals of $[Zn_4Fb_1]^{+}$, $[Zn_4Fb_1]^{+2}$, $[Zn_4Fb_1]^{+3}$, and $[Zn_4Fb_1]^{+4}$ are similar and qualitatively parallel the behavior observed for $[Zn_2]^{+}$. In particular, the signals for the cations of the pentameric arrays broaden slightly as the temperature nears the freezing point of the solvent and then broaden to a maximum, temperature independent width upon solvent freezing. However, unlike $[Zn_2]^{+}$, no hyperfine structure is resolved for the oxidized pentameric arrays at temperatures near the freezing point of the solvent. The frozen solution EPR line widths observed for both $[Zn_4Fb_1]^{+}$ and $[Zn_4Fb_1]^{+2}$ (~5.6 G) are similar to those observed for $[Zn_2]^{+}$ (~5.7 G) (cf. Figures 10 and 11 and Tables 2 and 3). The frozen solution line widths exhibited by $[Zn_4Fb_1]^{+3}$ and $[Zn_4Fb_1]^{+4}$ are narrower (~4.6 G). The temperature dependence observed for the EPR signals of $[Zn_4Fb_1]^{+5}$ deviates from the trend exhibited by the other four cations of this array. Although the signal initially broadens as the temperature nears the freezing point of the solvent, it then narrows upon solvent freezing rather than continuing to broaden. The frozen solution EPR line width observed for $[Zn_4Fb_1]^{+5}$ (~2.9 G) is slightly larger than that observed in liquid solution (~2.5 G). This behavior is qualitatively similar to that exhibited by $[Zn_1Fb_1]^{+2}$.

The temperature dependences observed for the EPR signals of the cation radicals of Zn_5 exhibit many features in common with those observed for Zn_4Fb_1, although there are some noteworthy differences. For example, the EPR signals of both $[Zn_5]^{+}$ and $[Zn_5]^{+2}$ broaden as the temperature nears the freezing point of the solvent and become still broader upon solvent freezing. No hyperfine structure is observed at any temperature. The frozen solution line width observed for $[Zn_5]^{+}$ is identical to that observed for $[Zn_4Fb_1]^{+}$ (~5.7 G), whereas the line width observed for $[Zn_5]^{+2}$ (~4.3 G) is somewhat narrower than that observed for $[Zn_4Fb_1]^{+2}$ (~5.5 G). The temperature dependence observed for the EPR signal of $[Zn_5]^{+5}$ also parallels that observed for $[Zn_4Fb_1]^{+5}$. The signal for $[Zn_5]^{+5}$ first broadens as the temperature nears the freezing point of the solvent and then narrows upon solvent freezing. However, unlike $[Zn_4Fb_1]^{+5}$, the frozen solution EPR signal for $[Zn_5]^{+5}$ is extremely narrow (~1.0 G) and significantly narrower than that observed at room temperature (~2.3 G). The narrowing observed for the EPR signals of $[Zn_5]^{+5}$ in frozen solution parallels the trend observed for $[Zn_2]^{+2}$. The temperature dependences observed for the EPR signals of $[Zn_5]^{+3}$ and $[Zn_5]^{+4}$ differ from those exhibited by $[Zn_4Fb_1]^{+3}$ and $[Zn_4Fb_1]^{+4}$ and are similar to those observed for $[Zn_5]^{+5}$ and $[Zn_2]^{+2}$. The signals for $[Zn_5]^{+3}$ and $[Zn_5]^{+4}$ first broaden as the temperature nears the freezing point of the solvent and then narrow upon solvent freezing. The line width of the frozen solution EPR signal for $[Zn_5]^{+3}$ (~2.5 G) is comparable to that observed at room temperature (~2.5 G); the line width for $[Zn_5]^{+4}$ (~1.2 G) is much less than that observed at room temperature (~2.3 G).

In order to gain further insight into the factors governing the temperature dependence of the EPR signals of the oxidized arrays, spectral data were acquired for certain monocations in DCB. The freezing point of DCB (258 K) is much higher than that of CH_2Cl_2 (176 K); therefore, data acquired in this solvent should provide a measure of the relative importance of changes in solvent state versus changes in temperature. The higher boiling point of DCB also allows the acquisition of solution phase data at elevated temperatures. EPR spectra were obtained in DCB at temperatures up to 380 K. The temperature range could not be extended further because the samples decompose rapidly at temperatures above 400 K.

The EPR spectra of $[Zn_1a]^{+}$, $[Zn_2]^{+}$, $[Zn_4Fb_1]^{+}$, and $[Zn_5]^{+}$ in DCB at 100, 295, and 380 K are shown in Figure 12. The temperature dependences of the hyperfine splittings or peak-to-peak line widths (when hyperfine structure is not resolved) are summarized in Table 4. The qualitative features observed in the EPR spectra of the different arrays in liquid and frozen DCB solutions are similar to those for CH_2Cl_2 solutions. The temperature dependent changes that occur in the spectral features are also similar in the two solvents. However, the pattern of

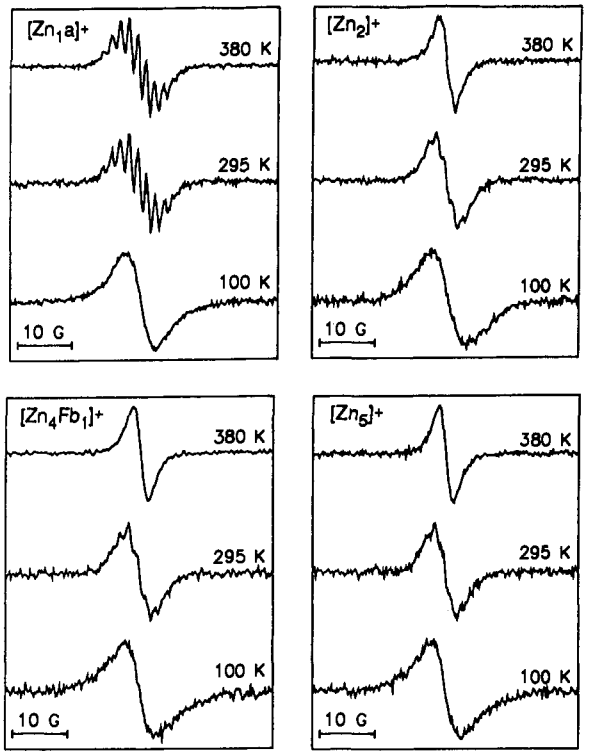

Figure 12. EPR spectra of $[Zn_1a]^+$, $[Zn_2]^+$, $[Zn_4Fb_1]^+$, and $[Zn_5]^+$ in DCB at 380, 295, and 100 K.

Table 4. Temperature Dependence of the Peak-to-Peak EPR Line Widths or Hyperfine Splittings (in Parentheses) for $[Zn_1a]^+$, $[Zn_2]^+$, $[Zn_4Fb_1]^+$, and $[Zn_5]^+$ in DCB[a]

T (K)	$[Zn_1a]^+$	$[Zn_2]^+$	$[Zn_4Fb_1]^+$	$[Zn_5]^+$
100	6.5	6.5	6.5	6.5
180	6.5	6.5	6.5	6.5
210	(1.6)	5.5	4.4	4.3
240	(1.6)	5.5	4.4	4.3
270	(1.6)	(1.4)	(1.3)	(1.3)
295	(1.6)	(1.4)	(1.3)	(1.3)
320	(1.6)	(1.4)	(~0.8)	(~0.8)
340	(1.6)	(1.4)	2.9	2.9
360	(1.6)	(1.4)	2.9	2.9
380	(1.6)	3.5	2.9	2.9

[a] Line widths and hyperfine splittings (G) are ±0.1 G.

spectral changes observed in DCB is shifted along the temperature axis commensurate with the difference in freezing point of the two solvents. More specifically, the signals observed for all the arrays in frozen DCB solutions are structureless and broad with line widths comparable to those observed for $[Zn_1a]^+$. At temperatures near the melting point of the solvent, the signals narrow and hyperfine structure is resolved. This structure is resolved for all the arrays in DCB, whereas structure is only observed for $[Zn_2]^+$ in CH_2Cl_2 (cf. Figures 10–12 and Tables 2–4). The hyperfine structure observed for $[Zn_2]^+$ persists up to high temperatures (~360 K) before it is lost due to line narrowing. The structures observed for $[Zn_4Fb_1]^+$ and $[Zn_5]^+$ collapse at lower temperatures (~330 K). The line widths observed for the structureless EPR signals of $[Zn_4Fb_1]^+$ and $[Zn_5]^+$ at elevated temperatures (~2.9 G) are less than those observed for $[Zn_2]^+$ (~3.5 G). However, the elevated temperature line widths for all the complexes in DCB are comparable to those observed at room temperature in CH_2Cl_2. These observations indicate that the features observed in the EPR spectra depend more strongly on the physical properties of the solvent (melting point, viscosity, etc.) than the temperature.

IV. Discussion

A major challenge in designing molecular photonic devices for light harvesting is to achieve electronic interactions among the pigments such that energy transfer prevails while avoiding electron-transfer quenching. Energy transfer occurs with about 90% efficiency in the diarylethyne-linked porphyrin arrays as determined by static fluorescence measurements; thus, competing singlet-state electron-transfer reactions do not occur in these compounds to a significant extent.[15a] These results appear consistent with a Förster mechanism of resonance energy transfer, though dynamic studies have not yet been done to determine whether the rates of transfer are faster than predicted in a Förster process. In noncovalently linked systems, resonance energy transfer has a R^{-6} dependence, where R is the center-to-center distance of the donor and acceptor.[38] For donors and acceptors at close distances, energy transfer can also occur via an electron exchange process. The rate of this process has an $e^{-2\beta R}$ dependence, where R is the donor–acceptor separation.[39] Electron-transfer reactions also have an exponential distance dependence.[40] The porphyrins in the arrays are held quite far apart by the diarylethyne linkers. However, the porphyrins are covalently linked and the diarylethyne linker is itself conjugated; consequently, the question arises whether the energy-transfer process may also involve electron exchange interactions mediated by the diarylethyne linker. Thus, it is essential to characterize all types of electronic communication in the arrays.

Two distinct types of electronic communication are of interest, through-space excitonic interactions and through-bond conjugative interactions. The through-bond conjugative interactions can involve electron exchange as well as spin exchange. The electrochemical and spectral properties of the arrays indicate that the electronic communication between the macrocycles is relatively weak in the ground and excited electronic states. The absorption characteristics of the arrays can be explained in terms of long-range, through-space excitonic interactions. Nevertheless, the electrochemical, RR, and EPR data indicate that through-bond electronic communication pathways are also open in the arrays (vide infra). Together these studies provide insight into the electronic communication mechanisms in the covalently-linked multi-porphyrin arrays. We begin by outlining the conformational dynamics of the arrays because these motions play a role in mediating the electronic communication. We then discuss excited-state electronic communication and finish with a description of ground-state communication.

A. Conformational Properties. There are four relevant sites where conformational motion can occur in the arrays: (1) *meso*-Tetraarylporphyrins can undergo macrocycle ruffling.[41] (2) For these porphyrins, rotation can occur about the *meso*-phenyl C–C bond. This rotation is somewhat hindered and the average dihedral angle in tetraphenylporphyrin is about 45°.[41] Rotation about the *meso*-aryl C–C bond of *o*-dimethylaryl units is substantially hindered, and coplanarity of the aryl and porphyrin rings cannot be achieved. (3) The rotational barrier about the ethyne bond in diphenylethyne has been calculated to be <1 kcal/mol.[42] (4) Ethynes are known to undergo bending; $C_{sp^3}–C_{sp}–C_{sp}$ bonds are easily distorted and have bending force constants about one-third of those for $C_{sp^3}–C_{sp^3}–$

(38) Förster, Th. *Ann. Phys.* **1948**, *2*, 55–75.
(39) Dexter, D. L. *J. Chem. Phys.* **1953**, *21*, 836–850.
(40) (a) Moser, C. C.; Keske, J. M.; Warncke, K.; Farid, R. S.; Dutton, P. L. *Nature* **1992**, *355*, 792–796 and references therein. (b) Paddon-Row, M. N. *Acc. Chem. Res.* **1994**, *27*, 18–25 and references therein.
(41) (a) Scheidt, W. R. In *The Porphyrins*; Dolphin, D., Ed.; Academic Press: New York, 1978; Vol. III, pp 463–512. (b) Meyer, E. F., Jr.; Cullen, D. L. *Ibid.* pp 513–530.
(42) Saebo, S.; Almlof, J.; Boggs, J. E.; Stark, J. G. *J. Mol. Struct. (THEOCHEM)* **1989**, *200*, 361–373.

C_{sp^3} bonds.[43] The pliability of the bonds in diarylethynes $C_{sp^2}-C_{sp}-C_{sp}$ is not known; however, it is reasonable that they would have greater rigidity than alkylethynes.

In work currently in progress,[44] we have measured the dipolar interactions[45] between adjacent protons in a selection of porphyrin arrays via high-field NMR techniques. The data have been used to infer some of the conformational properties of the arrays. The initial conclusions are that the barrier to rotation about the ethyne bonds is extremely small, probably 500 cal or less, and that bending (presumably at the ethyne linkage) results in a root-mean-square angle of 25 ± 4° between the in-plane axes of adjacent porphyrins. These experiments indicate the diarylethyne is substantially less pliable toward bending than are dialkylethynes.[43] Picosecond transient experiments are required in order to gain information about the role of rotation about the ethyne bond in the energy-transfer process.

B. Excited-State Electronic Communication. The porphyrin−porphyrin electronic interactions in the arrays are weak as manifested by their slightly red-shifted and/or split B-state absorption bands. These features are suggestive of long-range, through-space excitonic interactions whose magnitudes are at most a few hundred wavenumbers.[8a,10d,e,18-21] However, it is also possible that the perturbed B-state absorption features of the arrays arise partly (or wholly) from through-bond interporphyrin interactions. This latter possibility is supported by the observation that the RR intensity enhancements for ν_{aryl} and $\nu_{C\equiv C}$ are unusually large. RR studies on other types of tetraarylporphyrins have shown that ν_{aryl} generally exhibits very little intensity enhancement,[22] reflecting relatively poor communication between the aryl and porphyrin π-electron systems.[46] The communication is poor because steric interactions force the aryl and porphyrin rings into highly non-coplanar conformations.[41] Accordingly, the large RR intensities observed for ν_{aryl} in the diarylethyne porphyrins suggest that the phenyl ring bearing the ethyne group assumes a more coplanar conformation with the porphyrin macrocycle than is typically observed. This view is supported by the observation that ν_{aryl} of Zn_1a' exhibits a diminished and more typical RR intensity enhancement. The rotation of the aryl group of Zn_1a toward the porphyrin plane would increase the conjugation between the π-electron systems of the two rings. This enhanced conjugation would provide a mechanism for the observed RR enhancement of $\nu_{C\equiv C}$ which is conjugated with the π-system of the aryl ring. In the case of the arrays, the ethyne linker also provides a conduit to extend the conjugation pathway to an adjacent porphyrin ring. These arguments notwithstanding, the increased conjugation must be relatively small because the absorption spectra are only very slightly perturbed.

Electronic communication through an extended π network can occur in both the ground and excited electronic states.[47] In contrast, excitonic interactions are confined exclusively to the excited states.[18] The features observed in the absorption spectra do not provide a means of distinguishing ground- versus excited-state perturbations because these spectra reflect the difference in electronic structure between the two states rather than the explicit structure of either state. The B-state RR intensities are also dictated by structural differences in the ground versus excited electronic states.[48] These structural differences determine the magnitude of the Franck−Condon overlaps along particular vibrational coordinates. On the other hand, the vibrational frequencies of the molecule reflect its ground-state properties. The ground-state properties are also reflected by the redox behavior of the system. The observation that the vibrational frequencies and the redox potentials of the diarylethyne-substituted porphyrins and arrays are similar to those of Zn_1s suggests that the ground-state properties of the arrays are similar to those of monomeric porphyrins. Accordingly, the structural differences that are responsible for the increased RR enhancements of ν_{aryl} (and $\nu_{C\equiv C}$) must primarily occur in the excited electronic state(s). This is reasonable because the excited states are more diffuse than the ground state and should be preferentially stabilized by a more extended π-electronic structure. In this regard, the small RR intensity enhancements typically observed for ν_{aryl} in tetraarylporphyrins are generally attributed to an excited-state conformational change in which the aryl group becomes more coplanar with the porphyrin ring.[22a,b] The presence of the conjugated ethyne group should further stabilize the diffuse excited states. This additional stabilization provides the driving force for further reducing the torsional angle between the porphyrin and aryl rings. The fact that the RR activities of ν_{aryl} and $\nu_{C\equiv C}$ are greater in the cations than in the neutral arrays suggests that the torsional angles for the former complexes are smaller than those of the latter.

The RR intensities observed for ν_{aryl} and $\nu_{C\equiv C}$ at different excitation wavelengths indicate that these modes are coupled to the Q-state as well as the B-state. The Q-state RR intensity enhancements depend on the magnitude of Herzberg−Teller coupling between the Q- and B-states rather than on the Franck−Condon overlaps with the ground state.[48] The Q−B vibronic coupling in tetraarylporphyrins is strong along a number of porphyrinic vibrational coordinates.[49] Strong coupling produces complicated RR enhancement patterns with multiple maxima. These maxima do not necessarily reflect the vibrational frequencies of the molecule. The large RR enhancements observed for ν_{aryl} and $\nu_{C\equiv C}$ with excitation in the high-vibronic satellites of the Q-state indicate that the vibronic coupling for these modes is also extremely strong. This coupling indicates the presence of an ethyne-mediated relaxation channel between the B- and Q-excited-states.

The initial RR studies of Zn_1a' indicate that the extended excited-state conjugation in the diarylethyne-substituted porphyrins can be disrupted by introducing the substituents on the aryl group that force the porphyrin and aryl rings to maintain a more non-coplanar conformation. Consequently, arrays constructed with porphyrins bearing *o*-dimethylaryl (or more bulky) substituents can be used to test whether the extended conjugation has any influence on either the B-state absorption features or the fluorescence excitation and emission properties. Such studies will provide a definitive test of whether the excited-

(43) (a) Montgomery, L. K.; Applegate, L. E. *J. Am. Chem. Soc.* **1967**, *89*, 2952−2960. (b) Allinger, N. L.; Pathiaseril, A. *J. Comput. Chem.* **1987**, *8*, 1225−1231.

(44) Bothner-By, A. A.; Dadok, J.; Johnson, T. E.; Lindsey, J. S. Manuscript in preparation.

(45) (a) Bastiaan, E. W.; Maclean, C.; Van Zijl, P. C. M.; Bothner-By, A. A. In *Annual Reports on NMR Spectroscopy;* Academic Press: London, 1987; Vol. 19, pp 35−77. (b) Lisicki, M. A.; Mishra, P. K.; Bothner-By, A. A.; Lindsey, J. S. *J. Phys. Chem.* **1988**, *92*, 3400−3403.

(46) (a) LaMar, G. N.; Eaton, G. R.; Holm, R. H.; Walker, F. A. *J. Am. Chem. Soc.* **1973**, *95*, 63−75. (b) Walker, F. A.; Balke, V. L.; McDermott, G. A. *J. Am. Chem. Soc.* **1982**, *104*, 1569−1574.

(47) (a) Skotheim, T. A., Ed.; *Handbook of Conducting Polymers*; Marcel Dekker: New York, 1986; Vols. 1 and 2. (b) Chien, J. C. W. *Polyacetylene: Chemistry, Physics, and Materials Science*; Academic Press: Orlando, FL, 1984. (c) Brédas, J. L.; Chance, R. R. In *Conjugated Polymeric Materials: Opportunities in Electronics, Optoelectronics, and Molecular Electronics*; NATO ASI Series E, Vol. 182; Kluwer Academica Publishers: Boston, MA, 1990. (d) Tolbert, L. M. *Acc. Chem. Res.* **1992**, *25*, 561−568.

(48) (a) Johnson, B. B.; Peticolas, W. L. *Annu. Rev. Phys. Chem.* **1976**, *27*, 465−491. (b) Spiro, T. G.; Stein, P. *Annu. Rev. Phys. Chem.* **1977**, *28*, 501−521. (c) Felton, R. H.; Yu, N.-T. In *The Porphyrins*; Dolphin, D., Ed.; Academic Press: New York, 1978; Vol. III, pp 347−394. (d) Spiro, T. G. In *Iron Porphyrins*; Lever, A. P. B., Gray, H. B., Eds.; Addison-Wesley: Reading, MA, 1983.

(49) Shelnutt, J. A.; O'Shea, D. C. *J. Chem. Phys.* **1978**, *69*, 5361−5374.

state characteristics of the arrays are due to through-space or through-bond interactions.

C. Ground-State Electronic Communication. Our approach for assessing ground-state interactions in the arrays involved electrochemical formation of cation radicals and EPR studies. EPR studies of oxidized pigments in natural photosynthetic light-harvesting complexes have been performed in order to determine the number of pigments in electronic communication.[50] EPR data obtained for oxidized photosynthetic reaction centers provided the original evidence that the primary donor is a dimer.[51] In our case, the number of pigments is known and our studies measure energies, hole/electron hopping rates, and spin exchange interactions. In addition to providing information about electronic interactions related to energy-transfer processes, these studies have unveiled electronic properties of the arrays that are fascinating in their own right.

Although the inter-porphyrin interactions in the ground states of the diarylethyne-linked arrays are weaker than those in the excited states, ground-state communication is clearly reflected in the electrochemical and EPR data for the complexes. The electrochemical studies indicate that, while the one-electron redox potentials for the zinc units in Zn_2, Zn_4Fb_1, and Zn_5 are similar, they are not identical. The EPR spectra of the oxidized assemblies exhibit complex temperature dependent signatures that reflect inter-porphyrin interactions. All of these features can be explained by hole/electron hopping and/or spin exchange mechanisms.[52] In the cases of Zn_1Fb_1 and Zn_2, either one or the other mechanism is operative for a particular cation. This is also the case for certain cations of the pentameric arrays; however, for others, both mechanisms are simultaneously operative.

The fact that the EPR spectra of all the cations are independent of concentration indicates that the hole/electron hopping and exchange is intramolecular rather than intermolecular. The inter-porphyrin interactions in the assemblies must be mediated through the arylethyne bridges because the interring separations are extremely large. The edge-to-edge separations of nearest neighbors are ~13 Å. In the pentameric arrays, the closest approach edge-to-edge distance between peripheral units is ~20 Å. The rates of through-space hole/electron hopping or magnitude of spin exchange over such distances would be at least 10^8 times less than those observed for the arrays (vide infra).[40,52a] The rate of inter-porphyrin hole/electron hopping is slow on the electronic and vibrational time scales (10^{-13}–10^{-15} s); consequently, the absorption and RR spectra are a superposition of the spectra of the individual components. In contrast, the processes are fast or comparable to the relatively long time scales that determine the EPR signatures (10^{-6}–10^{-8} s); hence, the spectra deviate from simple superpositions.

In the following sections, we first discuss the hole/electron hopping and spin exchange interactions in the dimeric arrays. The fact that only one or the other of these processes is operative for a given oxidation state of the dimers makes the interpretation of the spectral data for these arrays less complicated than for the pentamers. We then discuss the pentameric arrays using the properties of the dimers as benchmarks.

(1) Dimeric Arrays. Both $[Zn_2]^+$ and $[Zn_2]^{+3}$ contain a single unpaired spin. If this spin density is localized on one center on the EPR time scale, then the hyperfine splittings and line widths would be similar to those observed for $[Zn_1a]^+$. On the other hand, if the hole/electron hops between the two porphyrins in the dimer, the hyperfine parameters will be modulated to an extent determined by the hopping rate.[52a] If the hole/electron is completely delocalized (rapid hopping) compared with the time scale reflected by the hyperfine splittings, the hyperfine coupling will be reduced by a factor of 2. In the case of unresolved hyperfine splittings, the peak-to-peak line width in a delocalized dimer is scaled by a factor of $2^{-1/2}$.[51] At intermediate hopping rates, the spectral features are more complicated.

The liquid solution EPR spectra of both $[Zn_2]^+$ and $[Zn_2]^{+3}$ are characterized by narrow lines with no resolved hyperfine structure (Figure 10, Table 2). Spectral simulations indicate that the observed line shapes are reproduced extremely well if the ^{14}N hyperfine coupling is halved (relative to $[Zn_1a]^+$) and the unpaired spin is allowed to interact with eight ^{14}N nuclei rather than four. Simulations in which the hyperfine coupling constant is reduced without changing the number of interacting nuclei do not satisfactorily account for the observed line shape. These results suggest that the hole/electron is delocalized over the two zinc porphyrin units in the dimer on the time scale of the hyperfine interactions. The ^{14}N hyperfine splittings observed for $[Zn_1a]^+$ are on the order of 1.6 G (4.5 MHz); consequently, the hole/electron hopping rates in $[Zn_2]^+$ and $[Zn_2]^{+3}$ must be on the order of 10^7 s^{-1} or greater but necessarily less than a typical vibrational frequency (10^{13}–10^{14} s^{-1}). In this regard, studies of covalently linked donor–acceptor complexes indicate that electron-transfer rates are on the order of 10^9 s^{-1} when the distances are comparable to the edge-to-edge interring separation of the dimeric arrays (~13 Å).[40] Regardless, the spectral characteristics exhibited by the pentameric assemblies suggest that the hole/electron hopping rates in $[Zn_2]^+$ and $[Zn_2]^{+3}$ are significantly faster than 10^9 s^{-1} (vide infra).

The frozen solution EPR spectra of $[Zn_2]^+$ and $[Zn_2]^{+3}$ are dramatically different from those observed in liquid solution and are similar to that observed for $[Zn_1a]^+$ (Figure 10, Table 2). This observation indicates that the rate of hole/electron hopping is slow on the EPR time scale in frozen solution. The EPR data acquired in CH_2Cl_2 versus DCB suggest that the state of the solvent rather than the temperature governs the hole/electron hopping. A variety of factors could mitigate the hole/electron-transfer process in frozen solution. These include solvent and/or counterion reorganization, oxidation-induced porphyrin reorganization, and conformational dynamics around the diarylethyne linkers.[6b] Additional studies are needed to determine which of these factors are most important.

$[Zn_2]^{+2}$ contains two spin centers, one on each unit of the dimer. Consequently, hole/electron hopping is not possible. On the other hand, the two spin centers can interact via long-range, through-bond exchange interactions (J).[52] EPR studies on a variety of biradicals have shown that through-bond exchange is effective over very long distances (15–25 Å) even when the spin centers are linked by a σ-bond network.[53,54] In the case where $J \sim 0$ or $J \ll a$, the observed spectrum is a superposition of the spectra of the two spin centers. If $J \gg a$, the observed spectrum exhibits hyperfine structure characteristic of interactions with two equivalent nuclei; the splittings between the lines are one-half those observed in the absence of exchange. In the intermediate exchange regime, a complex line shape is observed.[52]

The liquid solution EPR spectrum of $[Zn_2]^{+2}$ is similar to

(50) (a) Picorel, R.; Lefebvre, S.; Gingras, G. *Eur. J. Biochem.* **1984**, *142*, 305–311. (b) Gingras, G.; Picorel, R. *Proc. Natl. Acad. Sci. U.S.A.* **1990**, *87*, 3405–3409.

(51) Norris, J. R.; Uphaus, R. A.; Crespi, H. L.; Katz, J. J. *Proc. Natl. Acad. Sci. U.S.A.* **1971**, *68*, 625–628.

(52) (a) Atherton, N. M. *Principles of Electron Spin Resonance*; Ellis Horwood: New York, 1993; pp 253–263. (b) Bencini, A.; Gatteschi, D. *Electron Paramagnetic Resonance of Exchange Coupled Systems*; Springer Verlag: Berlin, 1990.

(53) Glarum, S. H.; Marshall, J. H. *J. Chem. Phys.* **1967**, *47*, 1374–1378.

(54) For a thorough discussion of exchange processes in biradicals, see: Closs, G. L.; Forbes, M. D. E.; Piotrowiak, P. *J. Am. Chem. Soc.* **1992**, *114*, 3285–3294.

those of $[Zn_2]^+$ and $[Zn_2]^{+3}$. In particular, the EPR signal of $[Zn_2]^{+2}$ is narrow and no hyperfine structure is resolved. Simulations of the EPR spectra indicate that the general features of the line shape can be approximately accounted for if the hyperfine coupling is halved and the spin system interacts with eight ^{14}N nuclei. This result qualitatively suggests that $J \gg a$ for $[Zn_2]^{+2}$. However, intermediate exchange cases cannot be ruled out with certainty because resolved features are not observed in the EPR spectra. In this regard, EPR studies of other biradicals linked by a σ-bond network indicate that J is on the order of 100−1000 MHz when the number of bonds between the spin centers is comparable to that in the dimeric arrays.[54] The value of J would be expected to be greater for the arrays because the spin centers are coupled via a π-bond network.

The EPR signals observed for $[Zn_2]^{+2}$ in frozen solution appear to be somewhat narrower than those observed in liquid solution. This observation suggests that the exchange mechanism is operative in frozen solution (unlike the hopping mechanism) and that exchange effects are more important in frozen than liquid solution. This could reflect a reduction in a^{14}_N, a larger value of J, or dynamical processes that modulate these parameters. In this regard, previous EPR studies of other biradicals have shown that J exhibits a complex temperature and solvent dependence.[53] For some solvents, J increases upon solvent freezing whereas for others it decreases. In certain solvents, no temperature dependence is observed. The detailed features of the J versus T plots also depend on solvent. For some solvents the plots are monotonic whereas for others, the plots exhibit a minimum. The various factors that mediate the temperature dependence of J are not certain. For the diarylethyne-linked porphyrins, J could be sensitive to a number of factors including solvent/counterion reorganization and/or macrocycle/linker conformation.

The large disparity in the redox potentials of the zinc and free base units of Zn_1Fb_1 precludes hole/electron hopping in either $[Zn_1Fb_1]^+$ or $[Zn_1Fb_1]^{+3}$. Consequently, the spectra of these complexes are similar to those of cations of monomeric zinc or free base porphyrins. In the case of $[Zn_1Fb_1]^{+2}$, exchange interactions can occur between the two spin centers in the biradical. The J-value for $[Zn_1Fb_1]^{+2}$ should be less than that for $[Zn_2]^{+2}$ due to the reduced overlap between the orbitals containing the unpaired spins.[55] The fact that the g- and a-values for the zinc and free base porphyrins are intrinsically different also influences how the exchange term effects the EPR line shape for $[Zn_1Fb_1]^{+2}$.[52,54] Exchange effects probably account for the fact that the line width of the liquid solution band contour of $[Zn_1Fb_1]^{+2}$ is slightly less than that observed for $[Zn_1Fb_1]^+$.

Interestingly, the frozen solution EPR line width observed for $[Zn_1Fb_1]^{+2}$ appears to be somewhat larger than that seen in liquid solution. This observation suggests that the magnitude of J is diminished in frozen solution. If so, solvent freezing has opposite effects on the J-values for $[Zn_1Fb_1]^{+2}$ and $[Zn_2]^{+2}$. It is difficult to rationalize a physical process that would produce such an effect. An alternative explanation is as follows: The relatively small J-value for $[Zn_1Fb_1]^{+2}$ dictates that the differences in the g- and a-values (Δg and Δa) for the zinc and free base units play a significant role in determining the detailed features of the EPR line shape. Conformational or other types of fluctuations (liquid solution) that reduce the dynamically averaged values of Δg and Δa would result in a narrower, better resolved spectrum. If these fluctuations are diminished (frozen solution), the intrinsic differences in the g- and a-values for the zinc versus free base units would be accentuated. This would tend to broaden the EPR signal and could overshadow the effect of increasing J in frozen solution.

(2) Pentameric Arrays. The features observed in the EPR spectra of all the cation radicals of Zn_5 and Zn_4Fb_1 can be explained by hole/electron hopping and/or spin exchange interactions. However, the detailed mechanism of these processes in the pentamers must be different from that in the dimers. In the case $[Zn_2]^+$ (and $[Zn_2]^{+3}$), hole/electron hopping occurs between adjacent spin centers and is mediated by the diarylethyne linker. In the cations of Zn_4Fb_1, hopping occurs between the peripheral zinc units and is mediated by the diarylethyne linker plus the intervening free base porphyrin. The hole does not reside on the core unit owing to its much higher oxidation potential. For the cations of Zn_5, the residency of the hole on the central zinc porphyrin depends on its redox potential relative to those of the peripheral units. The electrochemical studies on Zn_5 suggest that the fifth oxidation occurs at a potential somewhat higher than those of the first four. However, this potential reflects the energetics of removing a fifth electron from a tetracation. The energy required for this process is not necessarily the same as that required to place the hole of a mono (or other)-cation on the central zinc porphyrin versus a peripheral zinc unit.

In the cases of $[Zn_5]^+$ and $[Zn_4Fb_1]^+$, a single hole/electron hops among the zinc porphyrins and hopping is the only possible line narrowing mechanism. Simulations of the liquid solution EPR spectra of both complexes suggest that the hole is completely delocalized on the EPR time scale over at least four zinc porphyrins in the arrays. In particular, the EPR line shape for $[Zn_4Fb_1]^+$ is best reproduced if the hyperfine coupling is reduced by a factor of 4 and the unpaired spin is allowed to interact with 16 ^{14}N nuclei. The line shape observed for $[Zn_5]^+$ can be simulated by including either four or five centers. These two cases cannot be distinguished because the differences in line shape are too small. The hole/electron delocalizations that occur in $[Zn_4Fb_1]^+$ and $[Zn_5]^+$ indicate that the hopping rate is at least 10^7 s^{-1}. In frozen solutions, the EPR spectra of $[Zn_5]^+$ and $[Zn_4Fb_1]^+$ are broad and comparable in width to that of $[Zn_1a]^+$. This behavior is similar to that observed for $[Zn_2]^+$ and $[Zn_2]^{+3}$. These observations indicate that the rate of hole/electron hopping is slow on the EPR time scale for both $[Zn_5]^+$ and $[Zn_4Fb_1]^+$ in frozen solutions.

The fact that rapid hole/electron hopping occurs in $[Zn_4Fb_1]^+$ is remarkable given the presence of the intervening free base unit. The through-bond distance between adjacent peripheral porphyrins in $[Zn_4Fb_1]^+$ is more than twice that of the dimeric complexes and is at least 30 Å. An increase in separation by ~15 Å should reduce the rate of hole/electron transfer by a factor of $\sim 10^5$.[40] The fact that the hopping rate for $[Zn_4Fb_1]^+$ is at least 10^7 s^{-1} suggests that the processes in $[Zn_2]^+$ and $[Zn_2]^{+3}$ must be extremely fast and could approach 10^{12} s^{-1}. These extremely rapid hopping rates must be due to the presence of the arylethyne conjugative pathway between the porphyrin rings. This pathway appears to promote electronic communication between the macrocycles even though the extent of conjugation is relatively small.

In the highly oxidized pentamers $[Zn_4Fb_1]^{+4}$ and $[Zn_4Fb_1]^{+5}$, each zinc porphyrin contains a single hole and hole/electron hopping is not possible. Consequently, the EPR line shape must be governed exclusively by exchange interactions. The number of bonds between the peripheral porphyrins of the pentameric arrays is much larger than between the two porphyrins in the dimers. Consequently, the exchange coupling should be diminished. On the other hand, more through-bond exchange pathways are available in the pentameric arrays compared with

(55) Kahn, O.; Briat, B. *J. Chem. Soc., Faraday Trans. 2* **1976**, *72*, 268–281.

the dimers. The existence of multiple exchange pathways precludes any unique interpretation of the EPR spectra. Regardless, the fact that the liquid solution EPR spectra of both $[Zn_4Fb_1]^{+4}$ and $[Zn_4Fb_1]^{+5}$ are very narrow indicates that the exchange interactions are substantial (Figure 11, Table 3). For both cations, solvent freezing increases the line width, suggesting that the overall exchange interactions are decreased. Again, the existence of multiple exchange pathways precludes a unique interpretation of this effect. The freezing-induced line width increase observed for $[Zn_4Fb_1]^{+4}$ is less than that observed for $[Zn_4Fb_1]^{+5}$. This observation indicates that the exchange interactions in the latter complex are greater than in the former. This is reasonable because $[Zn_4Fb_1]^{+5}$ contains a spin center on the core porphyrin which provides a direct link to the peripheral units.

As is the case for $[Zn_4Fb_1]^{+4}$ and $[Zn_4Fb_1]^{+5}$, hole/electron hopping cannot occur in $[Zn_5]^{+5}$ because each porphyrin contains a single hole. Consequently, exchange interactions must govern the characteristics of the EPR line shape. In the case of $[Zn_5]^{+4}$, through-bond hole/electron hopping can occur only if the central zinc unit is included in the hopping pathway. The electrochemical data suggest that there could be a barrier to placing the hole on the core unit in $[Zn_5]^{+4}$. Nevertheless, the line widths of the EPR signals observed for both $[Zn_5]^{+4}$ and $[Zn_5]^{+5}$ in liquid solution are comparable and extremely narrow (Figure 11, Table 3). This observation suggests that some amount of spin density must reside on the central zinc porphyrin in the tetracation. In addition, the line widths for both $[Zn_5]^{+4}$ and $[Zn_5]^{+5}$ narrow upon solvent freezing, suggesting that the exchange interactions increase. This behavior parallels that observed for $[Zn_2]^{+2}$. The extent of line narrowing observed for $[Zn_5]^{+4}$ approaches that seen for $[Zn_5]^{+5}$. This further suggests that some amount of hole density must reside on the central porphyrin unit.

In the intermediate stages of oxidation represented by $[Zn_4Fb_1]^{+2}$, $[Zn_4Fb_1]^{+3}$, $[Zn_5]^{+2}$, and $[Zn_5]^{+3}$ (and possibly $[Zn_5]^{+4}$), both hole/electron hopping and exchange can occur simultaneously in liquid solutions. The spectral features observed for these cations suggest that both processes contribute to the observed EPR line shapes. All of these cations exhibit narrow lines comparable in width to those of $[Zn_4Fb_1]^{+}$ and $[Zn_5]^{+}$ (cf. Figures 10 and 11 and Tables 2 and 3). In the rapid hopping limit, the presence of multiple spin centers increases the number of holes per center. Accordingly, the hyperfine couplings in a delocalized multication should be larger than those in a delocalized monocation. The increased hyperfine splittings should be manifested in the EPR spectrum as resolved structure and/or broader lines. The fact that this is not observed for the di- and trications indicates that the exchange process must contribute to additional line narrowing. The line widths observed for $[Zn_4Fb_1]^{+2}$, $[Zn_4Fb_1]^{+3}$, $[Zn_5]^{+2}$, and $[Zn_5]^{+3}$ (and $[Zn_5]^{+4}$) in frozen solution provide a measure of the importance of the exchange process in these systems (presuming that hole/electron hopping does not affect the frozen solution line width). The frozen solution line widths observed for $[Zn_4Fb_1]^{+2}$ are essentially identical to those observed for $[Zn_4Fb_1]^{+}$, suggesting that the exchange interactions are negligible in $[Zn_4Fb_1]^{+2}$. On the other hand, line narrowing is observed for $[Zn_4Fb_1]^{+3}$, suggesting that the exchange process is turning on. This is probably due to the fact that the average number of bonds between the spin centers is smaller for $[Zn_4Fb_1]^{+3}$ than for $[Zn_4Fb_1]^{+2}$. The number of exchange pathways is also larger in $[Zn_4Fb_1]^{+3}$. The lines for both $[Zn_5]^{+2}$ and $[Zn_5]^{+3}$ are relatively narrow. The enhanced communication in these cations can be rationalized if some amount of hole density can reside on the central porphyrin.

V. Summary and Conclusions

The electrochemical and spectral properties of the diarylethyne-linked porphyrin arrays indicate that the electronic communication between the macrocycles is relatively weak in the ground and excited electronic states. The perturbations observed in the electronic spectra of the arrays can be explained in terms of long-range, through-space excitonic interactions. Nevertheless, the extremely large RR intensity enhancements observed for ν_{aryl} and $\nu_{C\equiv C}$ suggest that the presence of the ethyne group induces a conformational change that enhances the conjugation between the π-electron systems of the porphyrin ring and arylethyne group. This enhanced conjugation is greater in the excited state(s) than in the ground state. Regardless, through-bond electronic communication does occur in the ground state as is evidenced by long-range electron/hole hopping and spin exchange in the cation radicals of the assemblies.

Initial studies of Zn_1a' indicate that the extended conjugation in the diarylethyne porphyrins can be disrupted by introducing substituents on the aryl group that force the porphyrin and aryl rings to maintain a more non-coplanar conformation. Studies on arrays constructed from the sterically constrained porphyrins will determine how this disruption in conjugation alters the electronic communication (energy transfer, hole/electron hopping, spin exchange) between the macrocycles. Time-resolved absorption and emission studies have already been initiated on the dimeric and pentameric arrays used in the current work in order to probe directly the rates of energy transfer. Ultimately, these studies will be extended to the sterically constrained systems. Collectively, these data should provide a complete picture of the ground- and excited-state electronic communications in the arrays.

The molecular design of these light-harvesting arrays was built around the notion that the porphyrins must be brought close enough to permit rapid energy transfer but held sufficiently far apart to preclude competing electron-transfer quenching reactions. The center-to-center distance of ~20 Å provided by the diarylethyne linker provides this distance, which is larger than has been typical in many porphyrin-based model systems. Other features of the molecular design and synthesis include the incorporation of facial-encumbering groups in order to achieve enhanced organic solubility and the use of a building block strategy that enables precise definition of the metalation state of each porphyrin in an array. These features provide robust access to multi-porphyrin arrays that can be tailored in versatile ways.

The electrochemical and EPR studies, aimed at establishing fundamental information about light-harvesting properties, have unveiled electronic phenomena of profound interest in their own right. The ability to remove five electrons from the pentameric arrays indicates their possible application as controlled-potential electron reservoirs. The diphenylethyne linker that serves to hold the porphyrins at relatively fixed distances also provides weak electronic communication among the porphyrins of an array. The communication, albeit weak, still permits rather rapid hole/electron hopping processes. The rapid mobility of the hole in the oxidized pentamers indicates that arrays of similar design, if fashioned in a linear architecture, could function as molecular wires or as components of electron-transport chains.

Acknowledgment. This work was supported by Grants GM36243 (D.F.B.) and GM36238 (J.S.L.) from the National Institute of General Medical Sciences.